ISTITUTO NAZIONALE DI FISICA NUCLEARE
Laboratori Nazionali di Frascati

LNF-81/83

M. Basile et al. : A MEASUREMENT OF THE PROMPT $e^{\pm}$ PRODUCTION CROSS-SECTION IN PROTON-PROTON COLLISIONS AT $\sqrt{s}$ = 62.2 GeV

Estratto da :
Nuovo Cimento 65A, 421 (1981)

Servizio Documentazione
dei Laboratori Nazionali di Frascati

IL NUOVO CIMENTO VOL. 65 A, N. 4 21 Ottobre 1981

A Measurement of the Prompt $e^{\pm}$ Production Cross-Section in Proton-Proton Collisions at $\sqrt{s} = 62.2$ GeV.

M. BASILE, G. CARA ROMEO, L. CIFARELLI, A. CONTIN,
G. D'ALÍ, P. DI CESARE, B. ESPOSITO, P. GIUSTI, T. MASSAM,
F. PALMONARI, G. SARTORELLI, G. VALENTI and A. ZICHICHI

CERN - Geneva, Switzerland
Istituto di Fisica dell'Università - Bologna, Italia
Istituto Nazionale di Fisica Nucleare - Sezione di Bologna, Italia
Istituto Nazionale di Fisica Nucleare - Laboratori Nazionali di Frascati, Italia
Istituto di Fisica dell'Università - Perugia, Italia

(ricevuto il 24 Luglio 1981)

Summary. — A measurement of prompt $e^{\pm}$ production in proton-proton collisions at the CERN ISR, for a centre-of-mass energy $\sqrt{s} = 62.2$ GeV, in an angular range $\Delta\theta = 35°$ around 90° and over a transverse-momentum range $1.0\ \text{GeV/c} \leqslant p_T^* \leqslant 3.0\ \text{GeV/c}$ is reported.

1. – Introduction.

The invariant cross-sections for prompt electrons and positrons ($e^{\pm}$), produced in proton-proton interactions, in an angular range $\Delta\theta = 35°$ around 90° c.m. polar angle, and at $\sqrt{s} = 62.2$ GeV, has been measured, in a transverse-momentum range of $e^{\pm}$ from 1.0 to 3.0 GeV/c. The value of the $e^{\pm}$ fractional longitudinal momentum was $|x_F| = |2p_L/\sqrt{s}| \leqslant 0.03$.

The measurements reported in the present study were particularly relevant for our program of heavy-flavour search at the ISR. In fact the electron-to-pion e/π ratio, especially in the high-p_T range, is strictly correlated with the semi-leptonic decay of the heavy flavours produced at the ISR.

The interest of these measurements is, however, more general than our own experimental research programme, in which a detailed understanding of

the ratio e/π was essential. In fact, at $\sqrt{s} = 62$ GeV and at 90° only one experiment (1) had been performed; at a lower energy, $\sqrt{s} = 53$ GeV, again only one experiment (2) had been done, not in the 90° region, but at $\sim 30°$ c.m. polar angle, and for lower transverse momenta $p_T \leqslant 1$ GeV/c.

2. – Experimental apparatus.

The experiment was performed at the CERN ISR by using the upgraded Split-Field Magnet (SFM) detector, which has almost full solid-angle coverage for unidentified charged-particle detection. A system of auxiliary detectors placed around the SFM was used for trigger and particle identification purposes. As shown in fig. 1, the experimental set-up consisted of

i) a system of multiwire proportional chambers (MWPCs) (3), located inside the SFM poles' gap, to provide the momentum measurement for charged secondaries;

ii) a small multiwire proportional chamber with analogue read-out (« dE/dx » chamber) (4), placed near the vacuum chamber, to detect Dalitz and external-conversion e^+e^- pairs;

iii) six atmospheric-pressure Čerenkov counters (C0, C1, C2, C3, C4, C5) consisting of four cells each, to reject charged particles heavier than $e^\pm$;

---

(1) F. W. BÜSSER, L. CAMILLERI, L. DI LELLA, B. G. POPE, A. M. SMITH, B. J. BLUMENFELD, S. N. WHITE, A. F. ROTHENBERG, S. L. SEGLER, M. J. TANNENBAUM, M. BANNER, J. B. CHÈZE, H. KASHA, J. P. PANSART, G. SMADJA, J. TEIGER, H. ZACCONE and A. ZYLBERSTEJN: *Nucl. Phys. B*, **113**, 189 (1976).

(2) L. BAUM, M. M. BLOCK, B. COUCHMAN, J. CRAWFORD, A. DEREVSHCHIKOV, D. DIBITONTO, L. GOLUTVIN, H. HILSCHER, J. IRION, A. KERNAN, V. KUKHTIN, J. LAYTER, W. MARSH, P. MCINTYRE, F. MULLER, B. NAROSKA, M. NUSSBAUM, A. ORKIN-LECOURTOIS, L. ROSSI, C. RUBBIA, D. SCHINZEL, B. SHEN, A. STAUDE, G. TARNOPOLSKY and R. VOSS: *Phys. Lett. B*, **60**, 485 (1976); M. BARONE, M. BLOCK, A. BÖHM, F. CERADINI, D. DIBITONTO, J. IRION, A. KERNAN, J. LAYTER, F. MULLER, A. NAKKASYAN, B. NAROSKA, F. NAVACH, M. NUSSBAUM, A. ORKIN-LECOURTOIS, C. RUBBIA, M. SACHWITZ, D. SCHINZEL, H. SEEBRUNNER, B. SHEN, A. STAUDE, R. TIRLER, G. VAN DALEN, R. VOSS and R. WOJSLAW: *Nucl. Phys. B*, **132**, 29 (1978).

(3) R. BOUCLIER, G. CHARPAK, E. CHESI, L. DUMPS, H. G. FISCHER, H. J. HILKE, P. G. INNOCENTI, G. MAURIN, A. MINTEN, L. NAUMANN, F. PIUZ, J. C. SANTIARD and O. ULLALAND: *Nucl. Instrum. Methods*, **115**, 235 (1974); R. BOUCLIER, R. C. A. BROWN, E. CHESI, L. DUMPS, H. G. FISCHER, P. G. INNOCENTI, G. MAURIN, A. MINTEN, L. NAUMANN, F. PIUZ and O. ULLALAND: *Nucl. Instrum. Methods*, **125**, 19 (1975).

(4) H. FREHSE, F. LAPIQUE, M. PANTER and F. PIUZ: *Nucl. Instrum. Methods*, **156**, 87 (1978); H. FREHSE, M. HEIDEN, M. PANTER and F. PIUZ: *Nucl. Instrum. Methods*, **156**, 97 (1978).

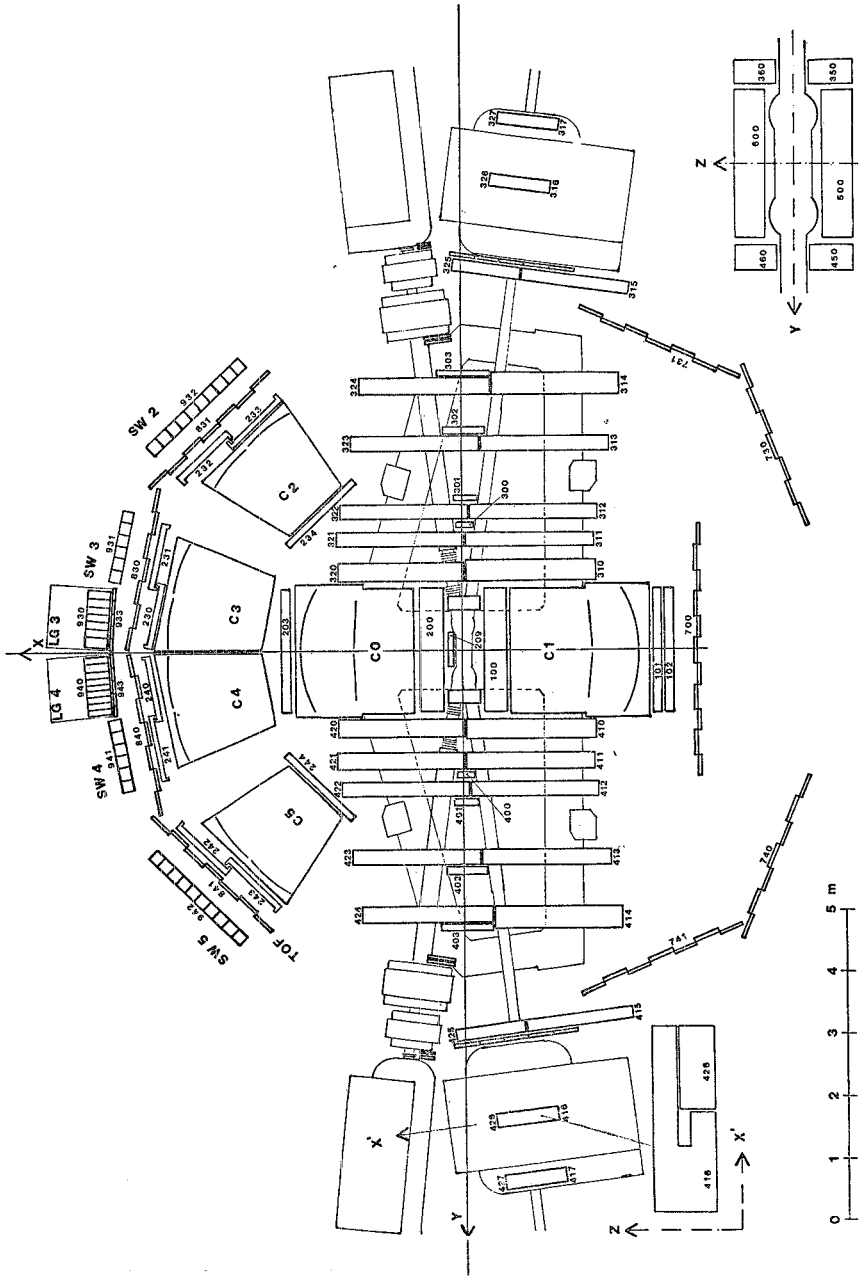

Fig. 1. – Top view of the SFM detector, showing the MWPCs and the external apparatus for particle identification: i) C0 to C5 are gas threshold Čerenkov counters, ii) SW2 to SW5 are lead/scintillator sandwiches, iii) LG3 and LG4 are lead-glass arrays, iv) TOF is the time-of-flight system, v) the chamber labelled « 209 » is the dE/dx chamber.

iv) four electromagnetic-shower detectors (EMSDs) [5] of the lead/scintillator sandwich type (SW2, SW3, SW4, SW5) to complement the Čerenkov selection and the SFM momentum measurement;

v) two electromagnetic-shower detectors (EMSDs) of the lead-glass total-absorption Čerenkov type (LG3, LG4) to cover the almost-zero-field region ($\theta_{c.m.} \simeq (90 \pm 5)°$) of the SFM, on the trigger side;

vi) extra multiwire chambers, in front of and behind the Čerenkov counters, to allow the reconstruction of charged-particle trajectories up to the electromagnetic-shower detectors;

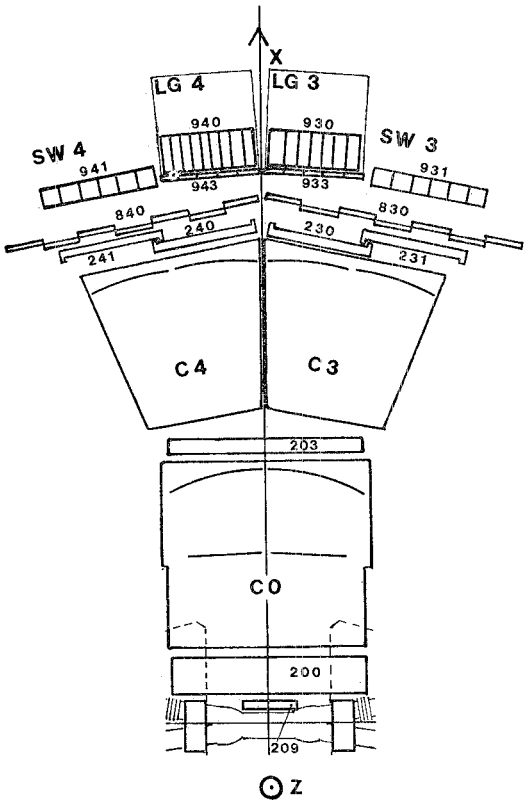

Fig. 2. – The detector region where the single-electron (SEL) trigger was required.

(5) M. BASILE, G. CARA ROMEO, L. CIFARELLI, A. CONTIN, G. D'ALÍ, P. GIUSTI, T. MASSAM, F. PALMONARI, G. SARTORELLI, G. VALENTI and A. ZICHICHI: *Nucl. Instrum. Methods*, **163**, 93 (1979).

vii) a time-of-flight system (TOF) ([6]) for the identification of charged particles up to ~ 2 GeV/c momenta.

The results presented in this paper refer to a set of data in which the prompt e± trigger was required in an interval of about $\pm 17.5°$ around $\theta_{c.m.} = 90°$, externally to the ISR ring (see fig. 2).

Notice that, since the proton-proton centre-of-mass system moved away from the trigger region with a velocity $\beta \simeq 0.152$, the transverse momenta of the e± in the centre-of-mass system were $\sim 12\,\%$ to $16.5\,\%$ (depending on the polar angle) larger than the momenta measured in the laboratory system.

A detailed description of the design and performances of the various elements of the set-up can be found elsewhere ([3-7]); in the following only a summary of the main characteristics of the detectors relevant to the prompt e± trigger will be given.

2·1. *Lead/scintillator sandwiches* (SW3, SW4). – Each of these telescopes consisted of six (200×20) cm² modules. Their sandwich structure was provided by a 1 cm thick lead plate followed by 10 layers of 1 cm thick scintillator interleaved with 9 plates of 0.4 cm thick lead. The total thickness of 8.2 radiation lengths was chosen such as to obtain an 80 % shower containment at 4 GeV e± energy. In the e± energy range from 0.5 to 4.0 GeV, the pulse-height response was linear with the energy within less than 5 % and, at 1 GeV, it corresponded to eight times the minimum ionizing charged-particle level; the uniformity of each module over its full surface was better than 3 % and the r.m.s. energy resolution was fitted by the formula

$$\frac{\sigma(E)}{E} = a + \frac{b}{\sqrt{E(\mathrm{GeV})}},$$

with the average parameter values $\langle a \rangle = 0.03$, $\langle b \rangle = 0.14$. For e± energies above 1 GeV a r.m.s. time resolution better than 0.32 ns and a r.m.s. space resolution, along the counter, better than 3 cm were obtained.

Concerning the π/e discrimination power of these counters, at 1 GeV and with an e± detection efficiency of 95 %, the pion contamination was 4 %.

During data taking, the stability of the energy calibration was monitored by triggering on penetrating particles across the central part of the modules. For this purpose, two scintillator counters (15 cm wide) were mounted on the back of each telescope at half height and matched its full horizontal width.

([6]) M. Basile, G. Cara Romeo, L. Cifarelli, A. Contin, G. D'Alí, P. Di Cesare, B. Esposito, L. Favale, P. Giusti, T. Massam, F. Palmonari, G. Sartorelli, G. Valenti and A. Zichichi: *Nucl. Instrum. Methods*, **179**, 477 (1981).

([7]) M. Basile, G. Cara Romeo, L. Cifarelli, A. Contin, G. D'Alí, R. Del Re, P. Giusti, T. Massam, F. Palmonari, G. Sartorelli, G. Valenti, R. Visco and A. Zichichi: CERN/ISRC/78-12, Geneva, 1 May 1978.

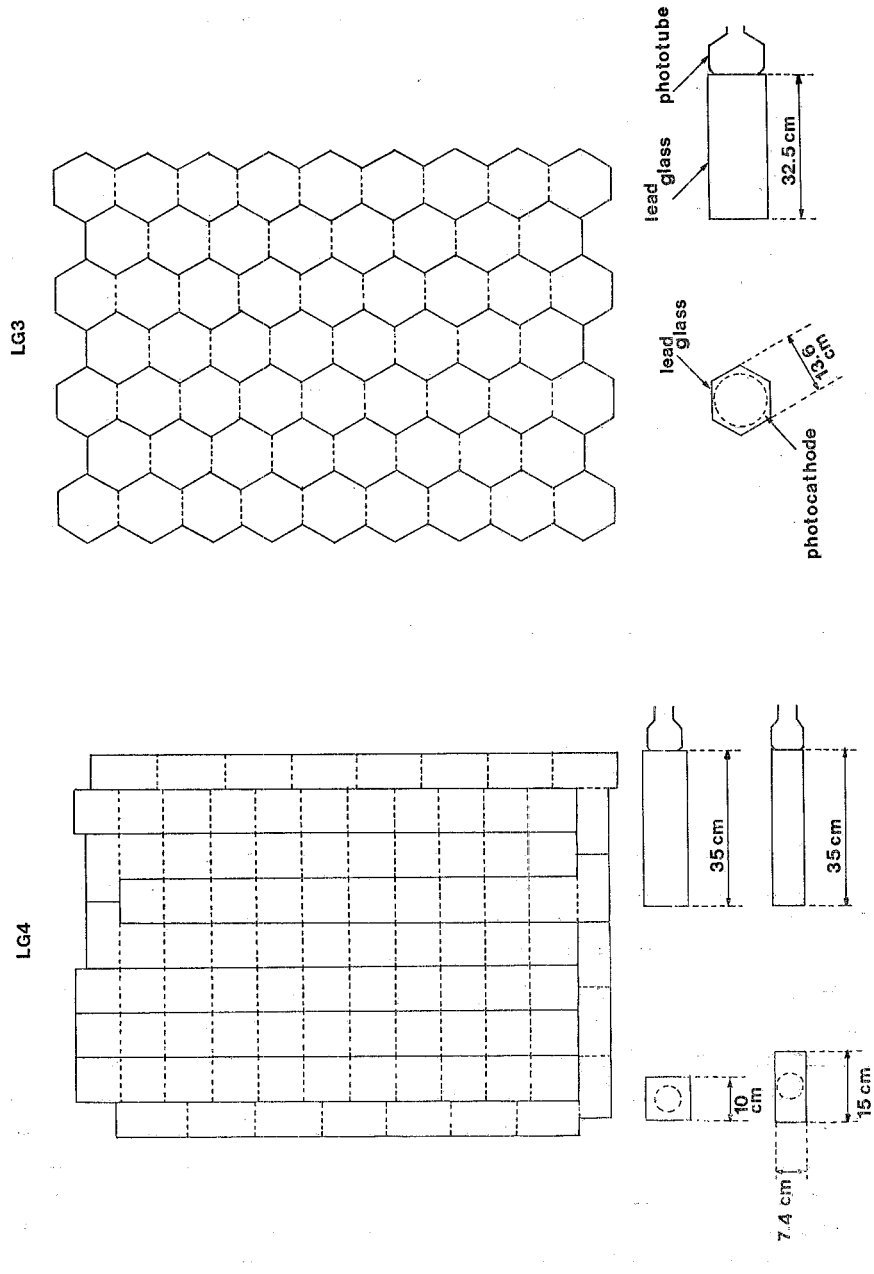

Fig. 3. – Front view of the two lead-glass arrays and details of the three types of lead-glass blocks.

2·2. *Lead-glass Čerenkov counters* (LG3, LG4). – The lead-glass array LG3 consisted of 60 hexagonal counters, each of inner diameter 13.6 cm and thickness 32.5 cm. LG4 consisted of 70 square counters (10×10) cm^2 plus 26 rectangular counters (15×7.4) cm^2 all of thickness 35 cm; see fig. 3. Each array covered an area of ~1 m^2 and was about 15 radiation lengths thick. The r.m.s. energy resolution for the two types of counters was fitted by the formula

$$\frac{\sigma(E)}{E} = a + \frac{b}{\sqrt{E(\mathrm{GeV})}},$$

with the following average parameter values:

$$\langle a\rangle = 0.030\,, \quad \langle b\rangle = 0.040 \qquad \text{for LG3;}$$

$$\langle a\rangle = 0.015\,, \quad \langle b\rangle = 0.048 \qquad \text{for LG4.}$$

In the $e^{\pm}$ energy range from 0.5 to 3.0 GeV, the pulse-height response of the counters was expressed by a parabolic behaviour with the quadratic-term coefficient smaller than 5% of the linear-term coefficient.

During data taking, the stability of the gain of each counter was monitored by three methods:

i) measurement of the spectrum produced by a radioactive source in a small scintillator installed in the centre of the front face of the counter;

ii) measurement of the spectrum produced by particles penetrating the lead-glass block and triggering one element (punch-through counter) of a scintillator hodoscope located behind each lead-glass array; a hodoscope of five scintillator counters placed just in front of the array was used in coincidence with the punch-through one;

iii) study of the invariant-mass spectrum of photon pairs of more than 0.7 GeV energy; the constancy of the peak value and of the full width of the observed π^0 mass spectrum (see fig. 4) was used as a monitor.

2·3. *Gas Čerenkov counters* (C0, C3, C4). – The Čerenkov counters C0, C3, C4 were filled with nitrogen and operated at atmospheric pressure; the pion momentum threshold was ~5.7 GeV/c.

Each of these counters was divided into four optical cells, each viewed by one photomultiplier (PM) whose window was treated with a wave-length shifter to increase the efficiency in the ultraviolet region. The light was collected by spherical mirrors and focused (after reflection on a second plane mirror for C0) on the photocathode of the relative PM (see fig. 5*a* and 5*b*). The optical system was designed bearing in mind the necessity to focus, on a relatively small surface (5 in tube), the light coming from a rather large source (interaction region + magnetic field); conical light catchers were used to increase the light collection efficiency.

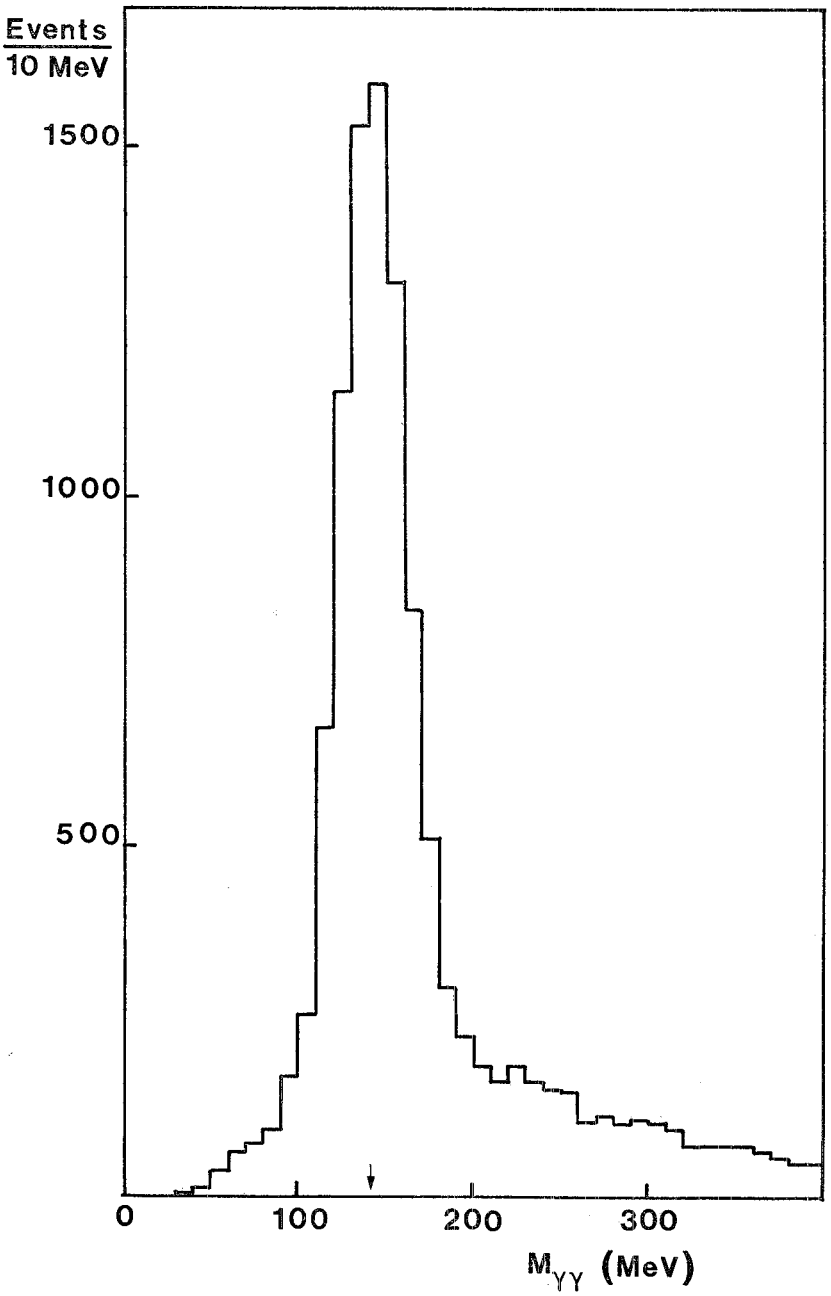

Fig. 4. – Invariant-mass spectrum of photon pairs with more than 0.7 GeV energy, obtained with the lead-glass arrays. The r.m.s. mass resolution at the π^0 peak is 14%.

As the SFM field could affect the efficiency of C0 phototubes, each of them was equipped with a set of three coils, inside the mu-metal shield, producing a magnetic field opposite to the one found in the photocathode region. A reference signal was provided by a light-emitting diode placed in the centre of the front end of the counter.

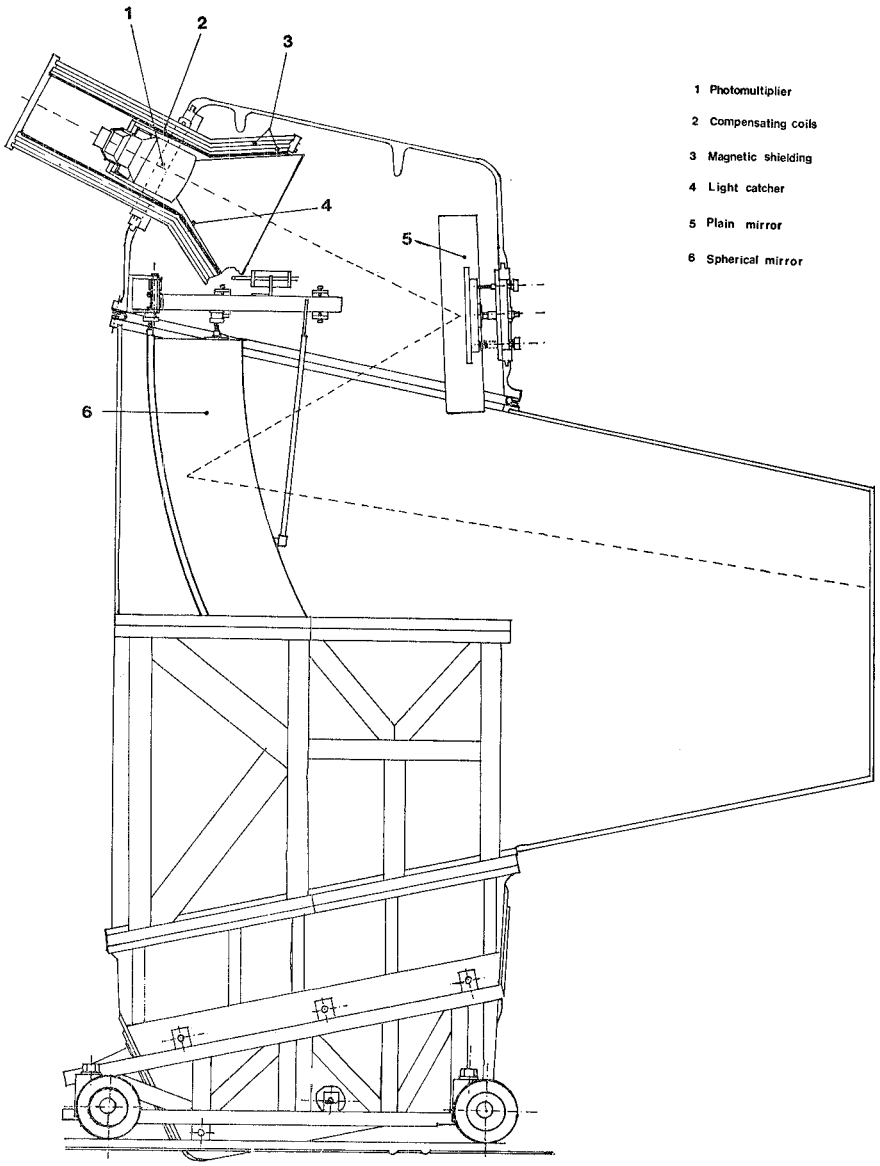

Fig. 5*a*. – Side view of the Čerenkov counter C0 showing the mechanical structure and the optical system.

A typical Čerenkov pulse-height response for an equal number of $e^{\pm}$ and pions of 2 GeV/c momentum obtained in a test beam is shown in fig. 5*c*; a Poisson fit to the $e^{\pm}$ spectrum gives 4.4 ± 0.1 as the average number of photoelectrons; to an $e^{\pm}$ efficiency $\geqslant 99\%$ corresponds a pion efficiency of about 0.8%.

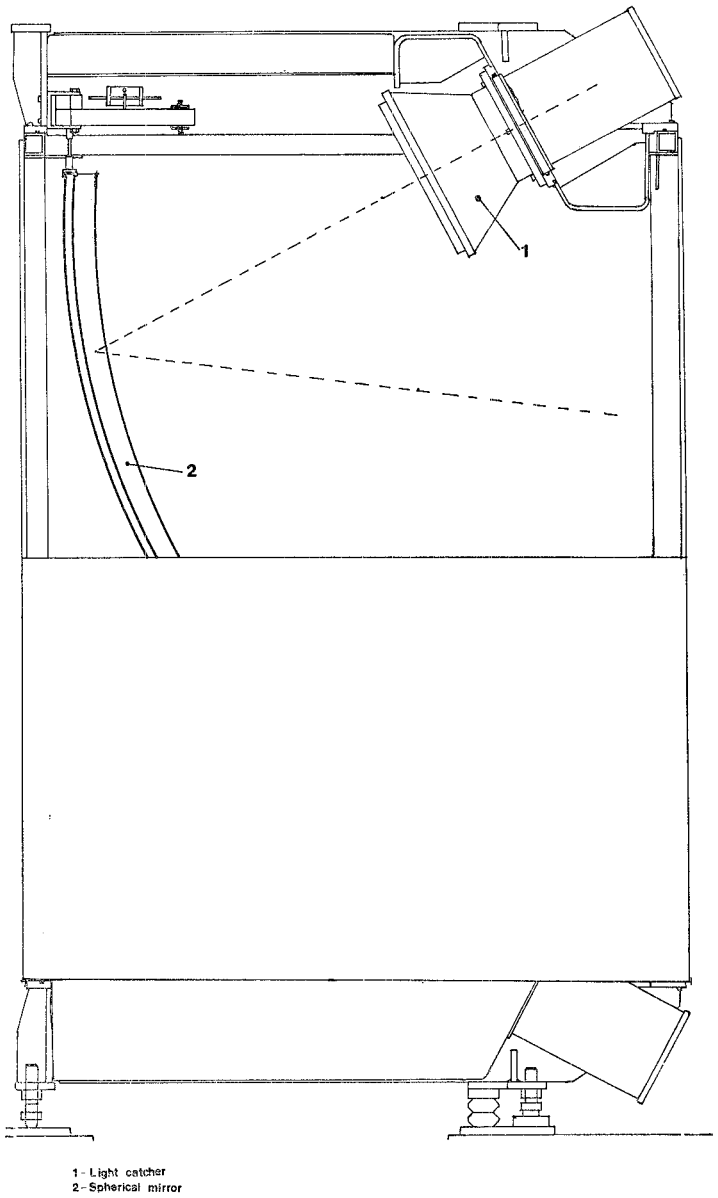

Fig. 5*b*. – Same as in 5*a* for Čerenkov counters C3 and C4.

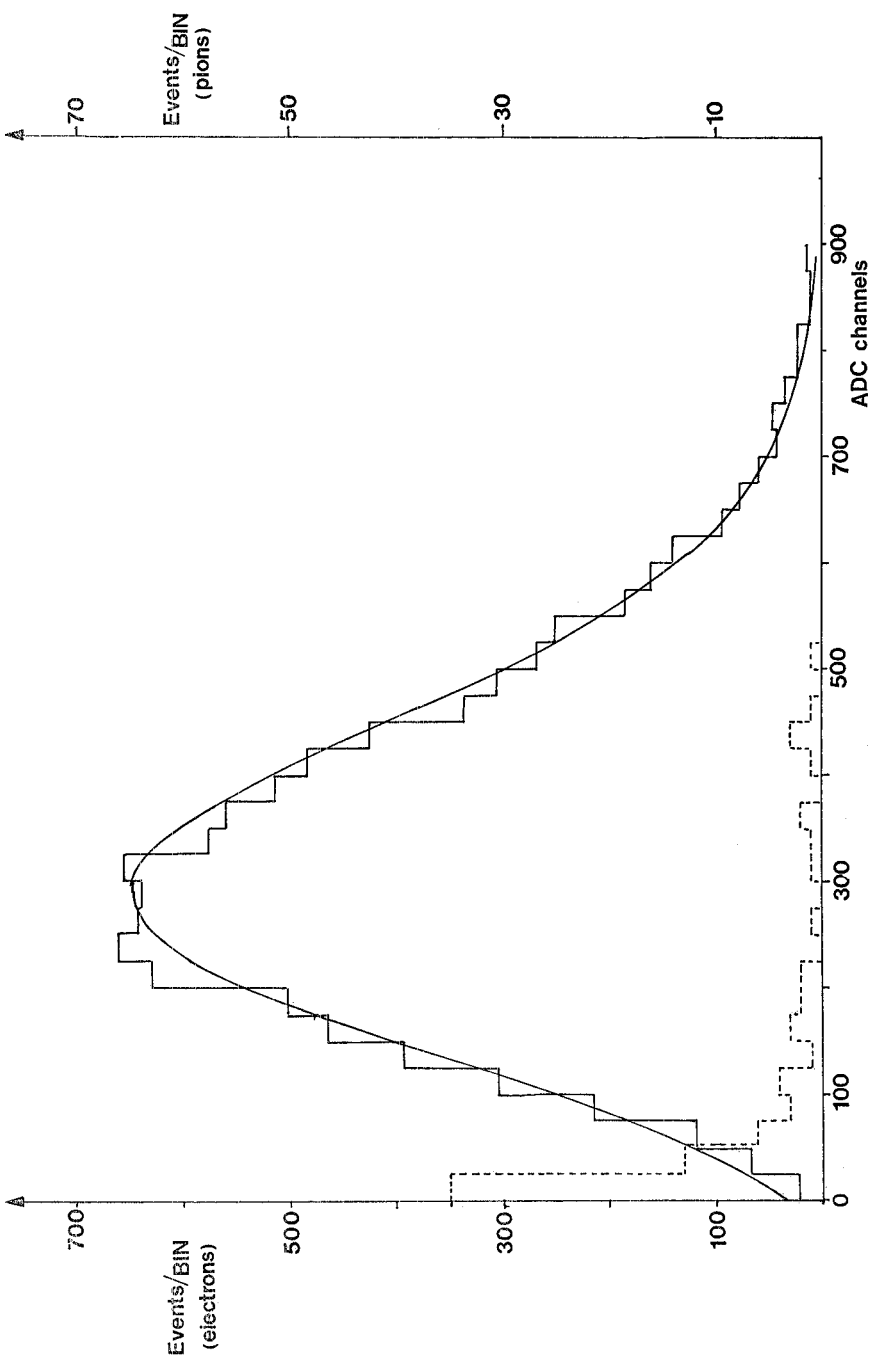

Fig. 5*a*. – Pulse-height spectrum of one of the Čerenkov counters, obtained in a test beam with equal numbers of electrons (full-line histogram) and pions (dashed-line histogram) of 2 GeV/*c* momentum.

2·4. dE/dx *chamber.* – This was a small ((57×27) cm^2 sensitive area) proportional chamber with three vertical and one horizontal wire planes with 4 mm spacing; each of the 493 wires had an independent analogic read-out channel (ADC). This chamber was located just outside the vacuum pipe (see fig. 1: chamber labelled « 209 ») and covered a solid angle of about 2 sr.

For each reconstructed track crossing the dE/dx chamber (fig. 2), the four energy loss samplings, corrected for impact angle and saturation effects, were used and an average loss was computed from the three lower pulse-height values. In fig. 6 the average pulse-height ($\overline{PH}$) distribution obtained with a

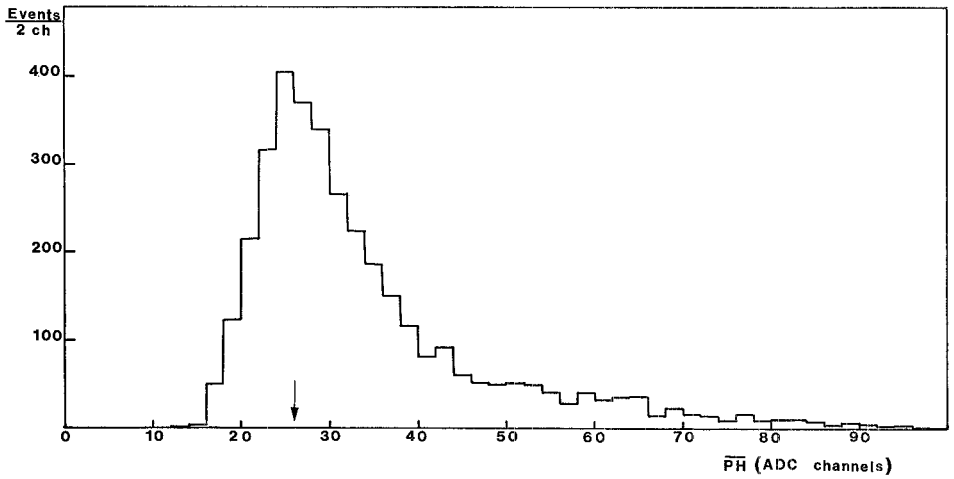

Fig. 6. – Average pulse-height ($\overline{PH}$) distribution of the dE/dx chamber obtained with the « pion » trigger for charged particles with momenta larger than 0.5 GeV/c. The arrow points to the most probable energy loss channel value. The FWHM resolution is about 50%.

« pion » trigger for momenta larger than 0.5 GeV/c is shown; the energy loss resolution is about 50 % FWHM. (The « pion » trigger was defined, as in the $e^{\pm}$ case (see sect. **3**), by a coincidence of MWPC and EMSD signals. To the latter, a « low threshold » condition, fully efficient for minimum-ionizing charged particles, was applied. No Čerenkov requirement was used at the on-line level.)

During the experiment, the gain stability of each channel was periodically monitored by injection of a fixed current pulse in the wire preamplifier. At the off-line level, corrections for small gain variations (a few per cent) were applied to the pulse-height value of each wire.

2·5. *The* ISR *vacuum chamber.* – It is finally worth mentioning the ISR vacuum chamber used in the pp interaction region where this experiment was mounted. In fact, a major design and engineering effort was needed to

reach a compromise between mechanical strength and wall thinness, the latter being an obvious requirement for an $e^{\pm}$ detection experiment.

The resulting chamber was a corrugated stainless-steel cylindrical pipe, 50 cm long, 24 cm in diameter and 0.2 mm thick.

When compared with the previous existing vacuum chamber, it represented an improvement by a factor of eight in the effective thickness traversed by $e^{\pm}$ and by a factor of two in the minimum distance of the first MWPC from the interaction region.

3. – $e^{\pm}$ trigger.

The single electron (SEL) trigger consisted of the electronic OR of four possible triggers (SEL/SW3, SEL/SW4, SEL/LG3, SEL/LG4), each corresponding to an $e^{\pm}$ candidate in one of the four EMSDs of fig. 2.

The standard trigger condition was defined by the following simultaneous requirements:

i) a signal from the Čerenkov counter C0;

ii) a signal from the Čerenkov counter C3 (for SEL/SW3 and SEL/LG3) or C4 (for SEL/SW4 and SEL/LG4);

iii) a fast signal from the wire planes of MWPCs « 200 » and « 203 » (see fig. 2);

iv) a fast signal from the wire planes of MWPCs « 230 » or « 231 » (for SEL/SW3), « 230 » (for SEL/LG3), « 240 » (for SEL/LG4), « 240 » or « 241 » (for SEL/SW4);

v) an energy deposition exceeding a given threshold in any module of a sandwich telescope or in any two adjacent columns of a lead-glass array; the nominal threshold values were 0.5 GeV for SW3, SW4 and 0.8 GeV for LG3, LG4.

More details about the electronic trigger logic can be found elsewhere [7].

4. – Data taking.

The measurements reported in this paper refer to a sample of $2.9 \cdot 10^6$ SEL triggers, corresponding to a total luminosity $\mathscr{L} = 4.39 \cdot 10^{36}$ cm^{-2}. At the beginning of each running period the luminosity was measured by using the SFM monitoring counter system and the Van der Meer method.

As already mentioned, during data taking special calibration runs were periodically intercalated in order to monitor the stability of all the electronic

channels connected to the various detectors (EMSDs, Čerenkovs, dE/dx chamber, MWPCs) and to check the energy calibration reference points of the EMSDs. Single and coincidence rates, together with pulse-height and time-of-flight spectra for each detector element, were continuously monitored.

With an average instantaneous luminosity $\langle L \rangle \simeq 0.9 \cdot 10^{31}$ cm^{-2} s^{-1}, the SEL trigger rate was about 6 s^{-1}, while the « pion » trigger rate was about $1.5 \cdot 10^{4}$ s^{-1}; a rejection factor against charged hadrons of about $2.5 \cdot 10^{3}$ was hence achieved on line by means of the « electron » requirements on the Čerenkov counters and the EMSDs.

5. – Data analysis.

The $2.9 \cdot 10^{6}$ collected events went through a fast off-line filtering process for a refinement of the trigger conditions and for a further rejection of the background caused by neutral and charged hadrons. The filter was based on the

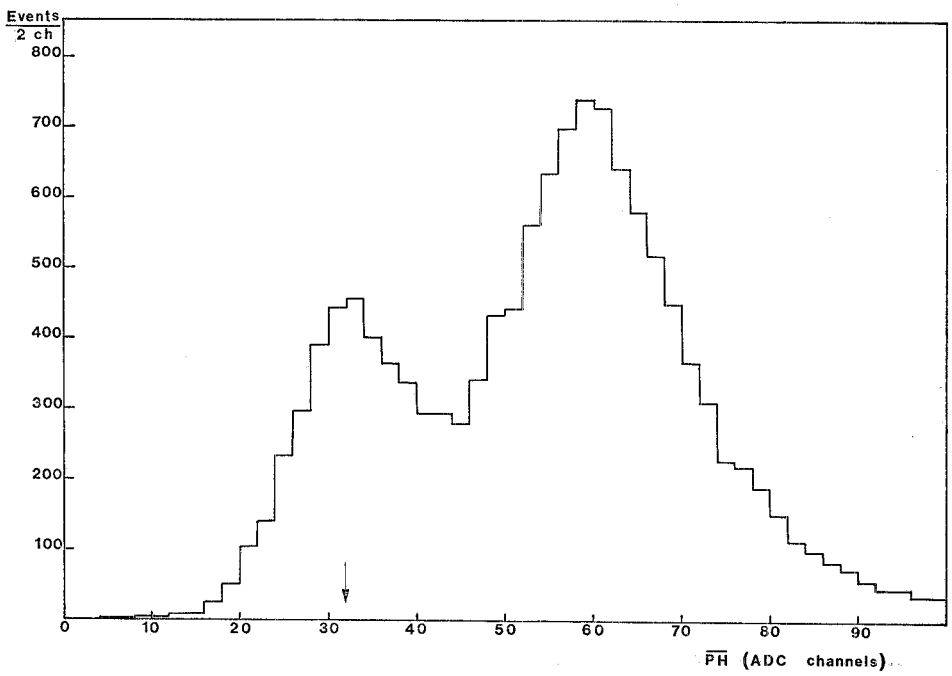

Fig. 7. – Average pulse-height ($\overline{\text{PH}}$) distribution of the dE/dx chamber obtained with the SEL trigger for tracks surviving the fast off-line filtering process (sect. **5**). The two peaks correspond to single- and double-particle (unresolved pairs) energy losses. The arrow points to the most probable energy loss channel value for the single-particle case.

following requirements:

i) the reconstruction of the trigger particle track in the MWPC telescopes of fig. 2, with a laboratory momentum larger than 0.5 GeV/c;

ii) the geometrical match of this track with

a) the Čerenkov counter cells,

b) the EMSD elements which had caused the trigger,

c) a set of four wire clusters, having a cluster size compatible with the crossing angle of the track, in the dE/dx chamber.

Only 15% of the input events survived the above off-line trigger criteria.

Since the main residual background sources for the prompt $e^{\pm}$ signal were Dalitz decays of high-momentum π^0 and η mesons, and conversions of high-momentum photons in the vacuum chamber wall or in the external foam frame of the dE/dx chamber, a search for the companion $e^{\pm}$ of the triggering one was made in the dE/dx chamber. In fact, the average pulse-height ($\overline{PH}$) distribution associated with the trigger track clearly showed (see fig. 7) a two-peak structure, corresponding to a single- and double-particle (unresolved pairs) ionization losses. Dalitz and external-conversion e^+e^- pairs were, therefore, rejected by requiring a $\overline{PH}$ value smaller than 1.4 times the most probable ionization loss of the prompt $e^{\pm}$.

The shape of the $\overline{PH}$ distribution of the single particle (fig. 6) was used to evaluate the efficiency of this cut for prompt $e^{\pm}$ detection (see table I) and the

TABLE I. – *Summary of prompt* $e^{\pm}$ *detection efficiencies.*

Selection applied	Efficiency
track finding and reconstruction (the efficiency, varying with p_T^* from 1 to 3 GeV/c is averaged over positive and negative electrons)	0.95 to 0.98 $\pm$ 0.01 (SW) 0.96 to 0.99 $\pm$ 0.01 (LG)
Čerenkov pulse-height cut (the efficiency is averaged over C0·C3 and C0·C4 PM combinations)	0.833 $\pm$ 0.004
track-energy cluster geometrical match	0.908 $\pm$ 0.01 (SW) 0.970 $\pm$ 0.01 (LG)
track-wire clusters (dE/dx chamber) geometrical match	0.944 $\pm$ 0.002
$\overline{PH} < 1.4 \times$ (prompt $e^{\pm}$ $\overline{PH}$ peak) cut in the dE/dx chamber	0.780 $\pm$ 0.009
angular cut of narrow resolved pairs	0.905 $\pm$ 0.002
geometrical match of energy and wire clusters after full reconstruction	0.896 $\pm$ 0.005
bad event format and full reconstruction event loss	0.934 $\pm$ 0.005
total	0.40 to 0.41 $\pm$ 0.01 (SW) 0.43 to 0.45 $\pm$ 0.01 (LG)

contamination level of narrow unresolved pairs in the surviving sample of events.

By inspection of the $\overline{\text{PH}}$ distributions for both the « pion » and the « electron » triggers, an approximate 25% increase of the most probable ionization

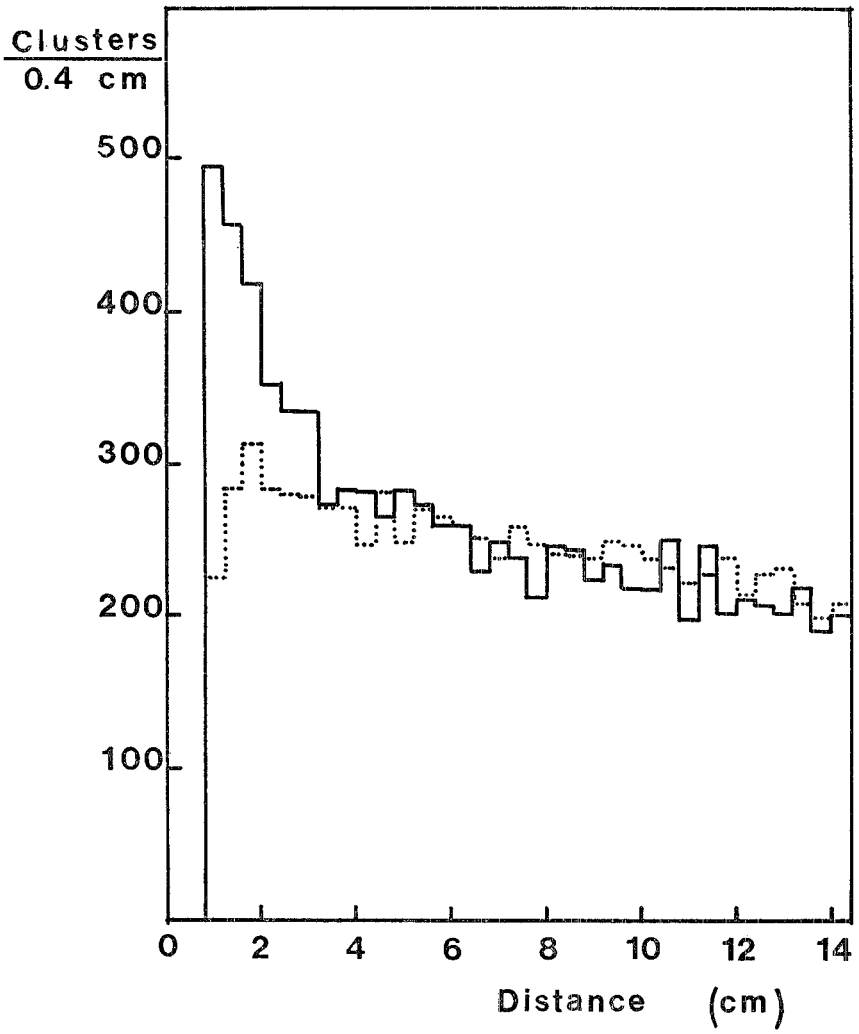

Fig. 8*a*. – Distribution of the minimum distance between the cluster associated with the $e^{\pm}$ trigger track and any other cluster in the same dE/dx plane for the SEL trigger (full-line histogram) and « pion » trigger (dashed-line histogram) events.

loss was observed for $e^{\pm}$ (at the Fermi plateau) with respect to minimum-ionizing particles. A fit to the lower end of fig. 7 using variable fractions of the « pion » and « electron » spectra showed that, once the above $\overline{\text{PH}}$ cut was applied, the pion contamination was less than 2%.

After having rejected the narrow unresolved e^+e^- pairs, a search was made in the dE/dx chamber for narrow resolved pairs. Owing to the Dalitz decay and external-conversion kinematics and to the high-transverse-momentum trigger condition, a very small opening angle or a largely asymmetric energy

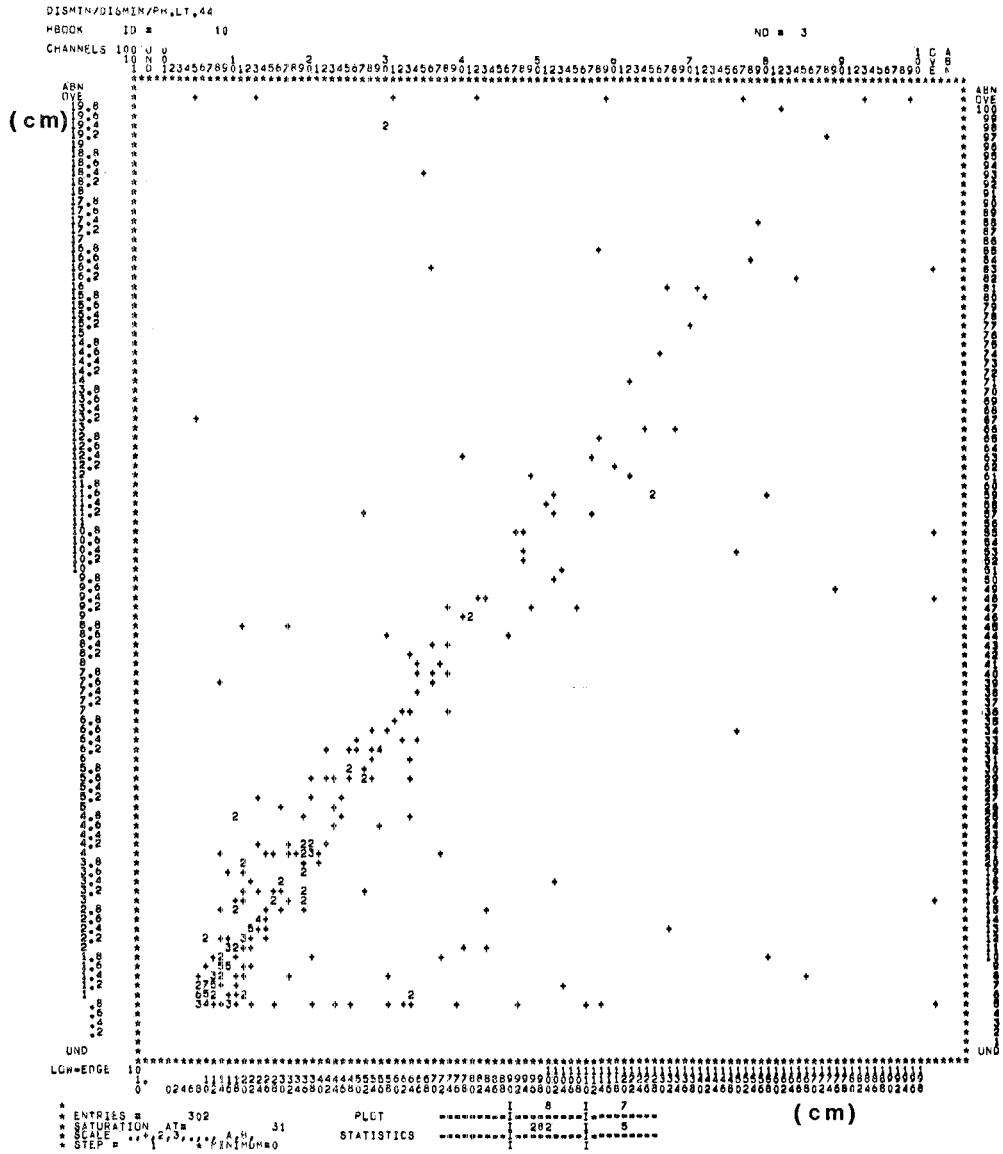

Fig. 8*b*. – Scatter plot of the minimum distance between clusters associated with the e± trigger track and any other cluster in the same dE/dx plane, for the first and the second plane of this chamber. Only events surviving the $\overline{\text{PH}}$ cut entered the plot. The same type of correlation was found for any two planes of the chamber.

sharing were expected for the e^+e^- pair. In both cases, the reconstruction (*i.e.* identification) of the two $e^\pm$ trajectories in the rapidly varying and largely inhomogeneous SFM magnetic field at $\sim 90°$ was very unlikely.

In fact, an excess of wire clusters in the dE/dx chamber, associated with a very-low-momentum track accompanying the trigger track, was found in the « electron » data when compared with the « pion » data (see fig. 8*a*). A correlation of the minimum distance between the clusters associated with the $e^\pm$ trigger track and any other cluster in the same dE/dx chamber plane, for any two planes, was observed (see fig. 8*b*).

Narrow but resolved e^+e^- pairs were then rejected by requiring, in each dE/dx chamber plane, no wire hit inside a correlation region of approximately 7° opening angle around the trigger track. From the « pion » trigger data the random vetoing effect of this cut was estimated to be 9.5%.

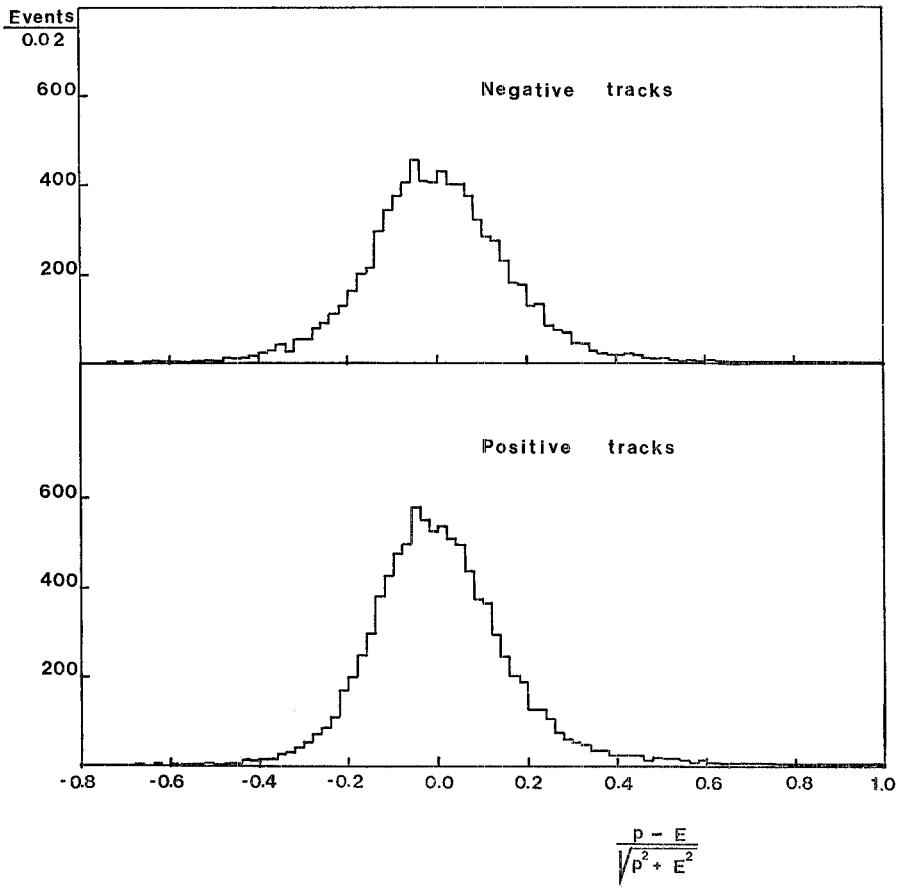

Fig. 9*a*. – $T = (p - E)/\sqrt{p^2 + E^2}$ distribution for a sample of $e^\pm$ candidates surviving the off-line filtering process.

The events satisfying all these cuts (1.7 % of the input events) were then fully reconstructed by using the whole system information of the SFM MWPCs. A very high charged multiplicity associated with the SEL trigger was found, its average value being 16.

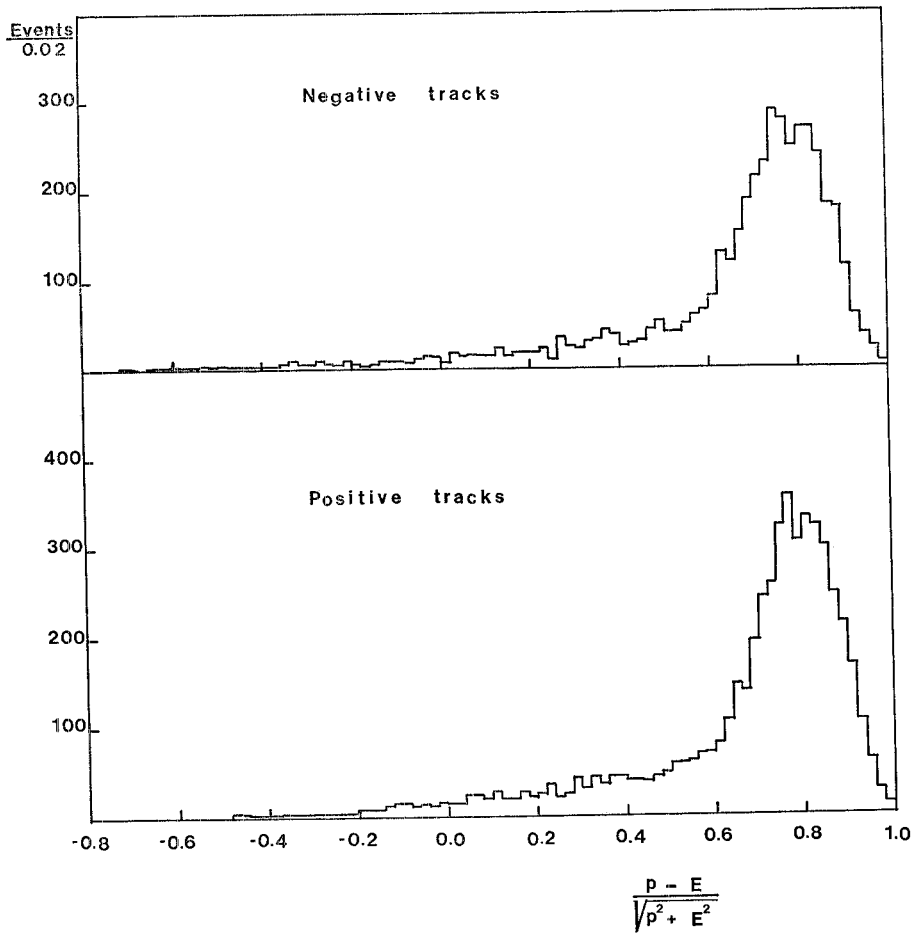

Fig. 9*b*. – Same as in 9*a* for a sample of « pion » trigger events.

The filtering process described above was then repeated on the trigger particle track found by the full reconstruction program; in fact, in a fraction of events (~ 10 %), this track did not coincide with that previously reconstructed by the faster but less accurate track-finding algorithm. Finally, this trigger track was required to originate from the interaction vertex, determined by all the reconstructed tracks of the event.

A further reduction of the charged-hadron background was achieved by comparing the behaviour of the momentum p (determined by the reconstruction program) with the energy E (measured by the EMSDs) of those trigger

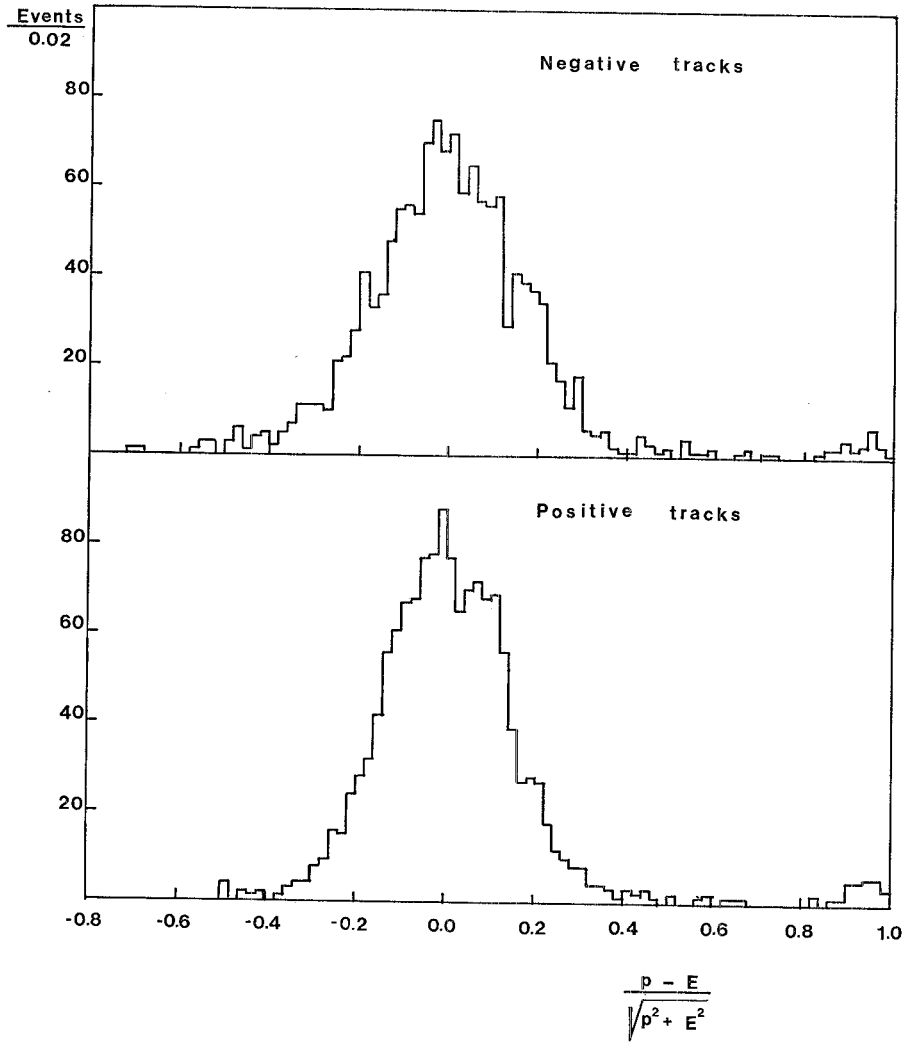

Fig. 9*c*. – Same as in 9*a* for a sample of SEL trigger events which were rejected by the $\overline{\text{PH}}$ cut.

particles traversing the « good » magnetic-field region ($\sim 80\,\%$ of the total). The quantity $T = (p - E)/\sqrt{p^2 + E^2}$ was used. Its distribution for the $e^{\pm}$ candidates (fig. 9*a*), while well centred on zero as expected for true $e^{\pm}$, showed

long tails both for positive and negative (*) values, the former being more populated than the latter.

The T distribution of the selected $e^{\pm}$ sample was compared with that of the « pion » trigger sample (fig. 9*b*) and with that of the rejected sample of high-$\overline{PH}$ tracks in the dE/dx chamber (fig. 9*c*). Notice that in fig. 9*c* the excess of events for $T > 0.8$ was due to slow particles below the minimum of ionization, releasing a large pulse height in the dE/dx chamber.

From the study of these three T distributions a maximum charged-hadron contamination of 2% was estimated; this value was in excellent agreement with that derived from the $\overline{PH}$ spectrum analysis.

$e^{\pm}$ candidates in the « good » magnetic-field region were, therefore, required to have a T value compatible with zero within three standard deviations ($\sigma_T = 0.13$); for those in the almost-zero-field region an equal amount of charged-hadron background was assumed and hence subtracted before computing the cross-section. After this T-distribution cut, the charged-hadron contamination was reduced to less than 1.5%.

A final sample of 45819 events was thus selected.

6. – Background determination.

In order to estimate the number of genuine prompt $e^{\pm}$ in the final sample of events, the background escaping the cuts of the filter (sect. **5**) had to be determined.

The main sources of this residual background were

i) Dalitz decays of π^0 and η mesons producing either very energy-asymmetrical e^+e^- pairs with the lower-momentum $e^{\pm}$ escaping detection in the dE/dx chamber or unresolved pairs giving a pulse height smaller than 1.4 times the most probable ionization loss of the prompt $e^{\pm}$;

ii) external conversions of photons in the vacuum chamber wall and in the external foam frame of the dE/dx chamber, producing e^+e^- pairs with the same characteristics as those from Dalitz decays;

iii) three-body semi-leptonic decays of charged and neutral kaons (K_{e3}) producing genuine but uninteresting (because of known origin) prompt $e^{\pm}$;

iv) prompt e^- from Compton scattering of high-momentum photons in the vacuum chamber wall or in the external foam frame of the dE/dx chamber.

(*) The background contribution to the negative-T region mainly came from antiproton annihilation in the EMSDs; by comparing the T distributions of positive and uegative particles (fig. 9*a*) an antiproton contamination of about 0.8% was evaluated.

The absolute number of background events, from each of the above sources, in each bin of centre-of-mass transverse momentum (p_T^*) was computed via a Monte Carlo program whose input data were

a) the British-Scandinavian Collaboration two-component function ([8]) to parametrize the p_T^* production spectra, at the ISR, of π^0 (taken as half the sum ([8]) of π^+ and π^- spectra), $K^\pm$ and K_L^0 (taken as half the sum ([9]) of K^+ and K^- spectra);

b) the η/π^0 production ratio measured at the ISR by the CCRS ([10]) and ABCS ([11]) Collaborations for p_T^* larger than 3 GeV/c and assumed to hold true also in the lower-p_T^* range of this experiment ($1 \leqslant p_T^* \leqslant 3$ GeV/c);

c) the known ([12]) branching ratios for the following decay processes: $\pi^0 \to \gamma\gamma$, $\eta \to \gamma\gamma$, $\pi^0 \to \gamma e^+e^-$, $\eta \to \gamma e^+e^-$, $K^\pm \to e^\pm \nu \pi^0$, $K_L^0 \to \pi^\pm e^\mp \nu$.

The contribution to the $e^\pm$ signal of the various background sources was then computed with the procedure described below.

6'1. $e^\pm$ *from Dalitz decays.* – The generation of π^0 and η mesons was done according to the parametrization and the relative rate mentioned above, in the centre-of-mass kinematical region corresponding to the SEL trigger:

a) (azimuthal angle) $\Delta\varphi^* = \pm 18°$, in the $(\hat{x}, \hat{z})$-plane, around the $\hat{x}$ axis of the SFM reference system (see fig. 1 and 2);

([8]) B. ALPER, H. BØGGILD, P. BOOTH, F. BULOS, L. J. CARROLL, G. DAMGAARD, G. VON DARDEL, B. DUFF, K. H. HANSEN, F. HEYMANN, J. N. JACKSON, G. JARLSKOG, L. JÖNSSON, A. KLOVNING, L. LEISTAM, E. LILLETHUN, E. LOHSE, G. LYNCH, G. MANNING, K. POTTER, M. PRENTICE, P. SHARP, S. SHARROCK, S. ØLGAARD-NIELSEN, D. QUARRIE and J. M. WEISS: *Nucl. Phys. B*, **100**, 237 (1975).

([9]) F. W. BÜSSER, L. CAMILLERI, L. DI LELLA, B. G. POPE, A. M. SMITH, B. J. BLUMENFELD, S. N. WHITE, A. F. ROTHENBERG, S. L. SEGLER, M. J. TANNENBAUM, M. BANNER, J. B. CHÈZE, H. KASHA, J. P. PANSART, G. SMADJA, J. TEIGER, H. ZACCONE and A. ZYLBERSTEJN: *Phys. Lett. B*, **61**, 309 (1976).

([10]) F. W. BÜSSER, L. CAMILLERI, L. DI LELLA, B. G. POPE, A. M. SMITH, B. J. BLUMENFELD, S. N. WHITE, A. F. ROTHENBERG, S. L. SEGLER, M. J. TANNENBAUM, M. BANNER, J. B. CHÈZE, J. L. HAMEL, H. KASHA, J. P. PANSART, G. SMADJA, J. TEIGER, H. ZACCONE and A. ZYLBERSTEJN: *Phys. Lett. B*, **55**, 232 (1975); F. W. BÜSSER, L. CAMILLERI, L. DI LELLA, B. G. POPE, A. M. SMITH, B. J. BLUMENFELD, S. N. WHITE, A. F. ROTHENBERG, S. L. SEGLER, M. J. TANNENBAUM, M. BANNER, J. B. CHÈZE, H. KASHA, J. P. PANSART, G. SMADJA, J. TEIGER, H. ZACCONE and A. ZYLBERSTEJN: *Nucl. Phys. B*, **106**, 1 (1976).

([11]) C. KOURKOUMELIS, L. K. RESVANIS, T. A. FILIPPAS, E. FOKITIS, A. M. CNOPS, S. IWATA, R. B. PALMER, D. C. RAHM, P. REHAK, I. STUMER, C. W. FABJAN, T. FIELDS, D. LISSAUER, I. MANNELLI, P. MOUZOURAKIS, A. NAPPI, W. J. WILLIS and M. GOLDBERG: *Phys. Lett. B*, **84**, 277 (1979).

([12]) R. L. KELLY, C. P. HORNE, M. J. LOSTY, A. RITTENBERG, T. SHIMADA, T. G. TRIPPE, C. G. WOHL, G. P. YOST, N. BARASH-SCHMIDT, C. BRICMAN, C. DIONISI, M. MAZZUCATO, L. MONTANET, R. L. CRAWFORD, M. ROOS and B. ARMSTRONG (PARTICLE DATA GROUP): *Rev. Mod. Phys.*, **52**, No. 2, Part II (1980).

b) (rapidity) $|y^*| < 0.7$, with $y^* = \frac{1}{2} \ln [(E^* + p_L)/(E^* - p_L)]$;

c) (transverse momentum) $p_T^* > 0.5$ GeV/c.

The normalization of the simulated background of $\pi^0(\eta)$ was derived from the total $\pi^0(\eta)$ production cross-section in that kinematical region (obtained by integration of the inclusive $\pi^0(\eta)$ invariant cross-section) and from the total integrated luminosity of the experiment. A vertex distribution reproducing the experimental diamond-shaped one was used. The e^+e^- Dalitz pairs were generated according to the known ([13]) invariant-mass and angular distributions of the $\pi^0(\eta)$ decay.

For those events in which at least one electron of the pair had a momentum larger than 0.5 GeV/c, the e± trajectories in the trigger region (fig. 2) were tracked up to the EMSDs, and the hit positions on the MWPC planes (dE/dx chamber included) were digitized. The pulse heights of the dE/dx chamber hit wires were also generated according to the experimental single-particle reference spectrum. After track reconstruction (with multiple scattering and energy loss taken into account), the Monte Carlo events went through a filtering analysis identical with the one applied to the data.

The p_T^* distribution of the surviving Dalitz e± was then parametrized according to the following formula:

$$\frac{dN}{dp_T^*} = A p_T^* \exp [-B p_T^*] + \frac{C}{(p_T^* + D)^E} .$$

The best-fit parameters (A, B, C, D, E) had different values for π^0 and η and, furthermore, A and C differed for positrons and electrons and for the four EMSD telescopes.

6'2. e± *from external conversions of photons.* – Experimental measurements on « direct » photon production at the ISR ([14]) show that at the centre-of-mass energy of this experiment no « direct » photon contribution is present below $p_T^* \simeq 3$ GeV/c. Only π^0 and η mesons decaying into two gammas were then considered as a source of conversion background.

The isotropic decay of these neutral mesons, generated with the same distribution and in the same kinematical region as for the Dalitz case, produced two photons, one of which, at least, was required to have an energy larger than

---

([13]) R. H. DALITZ: *Proc. R. Soc. London Ser. A*, **64**, 667 (1951); N. M. KROLL and W. WADA: *Phys. Rev.*, **98**, 1355 (1955); D. W. JOSEPH: *Nuovo Cimento*, **16**, 997 (1960).

([14]) For an extensive review of the data, see the session organized by L. RESVANIS: *Proceedings of the XX International Conference on High-Energy Physics, Madison, Wisconsin, 1980*, edited by L. DURAND and L. G. PONDROM, Part 1 (New York, N. Y., 1981), p. 133.

0.5 GeV. The probability of photon conversion into an e^+e^- pair, occurring either in the ISR vacuum chamber wall (0.2 mm thick) or in the foam frame (1 cm thick) of the dE/dx chamber, was computed by using known [15] e^+e^- pair energy-sharing and angular distributions. The effective thickness of material along the photon trajectory, and in particular the corrugation of the vacuum chamber wall, was carefully simulated in the Monte Carlo calculation.

For each electron of the pair the same tracking and filtering procedure as for the Dalitz case was applied. The p_T^* distribution of the accepted conversion $e^\pm$ was parametrized according to the same kind of formula as for the Dalitz $e^\pm$.

An independent evaluation of the absolute level of the residual conversion background in the final $e^\pm$ sample was derived from the same experimental data; a good agreement with the results of the Monte Carlo calculations was obtained (see appendix A).

6·3. $e^\pm$ *from* K_{e3} *decays.* – Charged and neutral (K_L^0) kaons were also generated with the above-mentioned distributions and kinematical cuts and allowed to decay semi-leptonically via the standard matrix element. The decay probability was constrained by the on-line and off-line requirements that the decay occurred before the first Čerenkov counter (C0) (for $K^\pm$) or the first dE/dx chamber plane (for K_L^0).

After the parent kaon and its decay $e^\pm$ were tracked through the detector telescopes of fig. 2, they were required to be reconstructed as a unique track.

The p_T^* distribution of such $e^\pm$ surviving the filtering analysis was parametrized by the following formula:

$$\frac{dN}{dp_T^*} = A_1 \exp\left[-Bp_T^*\right] + A_2 \frac{(1 - p_T^*/p_{beam})^m}{(p_T^{*2} + M^2)^n},$$

where $p_{beam} = 31.11$ GeV/c, $B = 8.24$ (GeV/c)$^{-1}$, $M = 1.0$ GeV/c and $n = 4.0$; the other parameters were assigned different values for positrons and electrons and for the four EMSD telescopes.

6·4. *Electrons from Compton scattering.* – The contribution from π^0 and η decay into two photons to the prompt (negative charge) electron signal, due to Compton scattering of the photons in the vacuum chamber wall or in the foam frame of the dE/dx chamber, was evaluated by using the Sternheimer [16]

---

[15] B. ROSSI: in *High-Energy Particles*, Chapter 2 (New York, N. Y., 1952), p. 79; R. M. STERNHEIMER: in *Nuclear Physics, Methods of Experimental Physics*, Vol. **5** A (New York, N. Y., 1961), p. 1.

[16] R. M. STERNHEIMER: *Phys. Rev.*, **99**, 277 (1955).

and the Klein-Nishina ([17]) formulae to integrate over the $\pi^0(\eta)$ and the photon energy spectra in the e± trigger region. The absolute invariant cross-section as a function of p_T^* relative to this type of background is given in table II.

The fractional contribution of the studied background sources to the experimentally observed e± signal is shown in fig. 10, as a function of p_T^*.

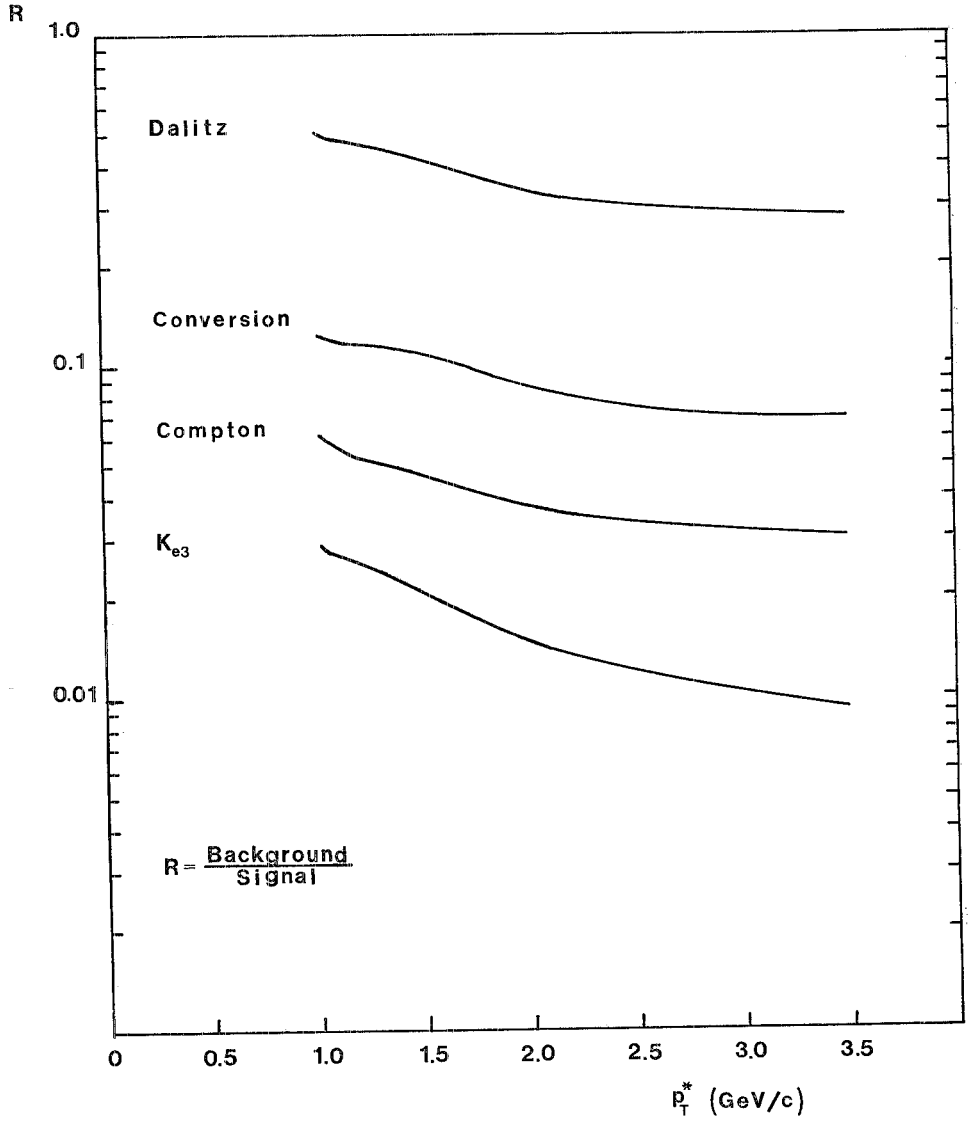

Fig. 10. – Ratio of the Monte Carlo e± background to the experimentally observed e± signal, after the off-line filtering process, as a function of p_T^*.

([17]) O. KLEIN and Y. NISHINA: *Z. Phys.*, **52**, 853 (1929), and references given in ref. ([15]).

TABLE II. – *The invariant cross-section for Compton* e^- *production as a function of* p_T^*.

p_T^* (GeV/c)	$E\,d^3\sigma/dp^3$ $(cm^2/(GeV)^2)$	p_T^* (GeV/c)	$E\,d^3\sigma/dp^3$ $(cm^2/(GeV)^2)$
1.022	$1.360 \cdot 10^{-32}$	1.973	$0.104 \cdot 10^{-33}$
1.072	$0.996 \cdot 10^{-32}$	2.041	$0.784 \cdot 10^{-34}$
1.122	$0.736 \cdot 10^{-32}$	2.142	$0.519 \cdot 10^{-34}$
1.172	$0.548 \cdot 10^{-32}$	2.242	$0.350 \cdot 10^{-34}$
1.222	$0.411 \cdot 10^{-32}$	2.342	$0.238 \cdot 10^{-34}$
1.272	$0.310 \cdot 10^{-32}$	2.442	$0.164 \cdot 10^{-34}$
1.322	$0.236 \cdot 10^{-32}$	2.542	$0.114 \cdot 10^{-34}$
1.372	$0.180 \cdot 10^{-32}$	2.642	$0.799 \cdot 10^{-35}$
1.422	$0.139 \cdot 10^{-32}$	2.743	$0.564 \cdot 10^{-35}$
1.472	$0.107 \cdot 10^{-32}$	2.843	$0.404 \cdot 10^{-35}$
1.522	$0.830 \cdot 10^{-33}$	2.943	$0.291 \cdot 10^{-35}$
1.572	$0.648 \cdot 10^{-33}$	3.043	$0.212 \cdot 10^{-35}$
1.623	$0.506 \cdot 10^{-33}$	3.143	$0.155 \cdot 10^{-35}$
1.673	$0.399 \cdot 10^{-33}$	3.294	$0.979 \cdot 10^{-36}$
1.723	$0.316 \cdot 10^{-33}$	3.597	$0.408 \cdot 10^{-36}$
1.773	$0.252 \cdot 10^{-33}$	3.900	$0.178 \cdot 10^{-36}$
1.823	$0.200 \cdot 10^{-33}$	4.202	$0.821 \cdot 10^{-37}$
1.873	$0.161 \cdot 10^{-33}$	4.504	$0.392 \cdot 10^{-37}$
1.923	$0.129 \cdot 10^{-33}$	4.806	$0.194 \cdot 10^{-37}$

7. – Acceptance and efficiency.

The $e^{\pm}$ acceptance of the apparatus was studied by tracking Monte Carlo simulated particles in the SFM magnetic field and by requiring each track to hit all the detectors (dE/dx chamber, Čerenkov counters, MWPCs, EMSDs) involved in the on-line $e^{\pm}$ trigger (see fig. 2). The $e^{\pm}$ were generated with a flat rapidity distribution and with an azimuthal angle and a transverse momentum within the allowed kinematical region of the trigger. Multiple scattering and energy loss in the various materials along the $e^{\pm}$ trajectory were duly taken into account.

The prompt $e^{\pm}$ effective acceptance, integrated over transverse momenta and averaged over the two electric-charge states, turned out to be $1.06 \cdot 10^{-2}$, while the purely geometrical acceptance, due to the solid angle subtended by the detector, was $1.5 \cdot 10^{-2}$. The shape of this acceptance for positive and negative electrons in the two types of EMSDs is given in fig. 11 as a function of p_T^*. The efficiency of the analysis was then evaluated step by step.

The efficiency of track finding and reconstruction in the trigger region was computed by simulation, and its behaviour as a function of p_T^* was determined; its value varied from 0.95 to 0.98, increasing with p_T^*, for $p_T^* \geqslant 1.0$ GeV/c.

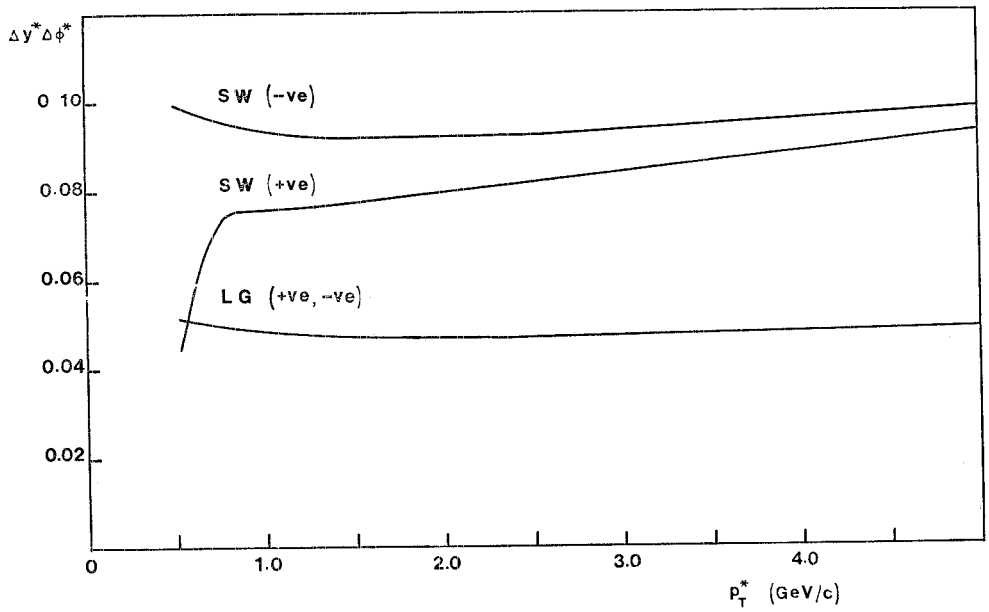

Fig. 11. – Prompt e± acceptance (in terms of the effective rapidity times the azimuthal-angle acceptance) as a function of p_T^*, for the two charge states and the two types of EMSDs; SW stands for SW3+SW4, LG for LG3+LG4.

The Čerenkov efficiency was evaluated by using the final sample of SEL triggered events. A Poissonian fit to the spectrum of each Čerenkov PM provided the mean number of observed photoelectrons. From these numbers, the efficiency to detect e± producing a pulse height larger than the hardware threshold (which corresponded to about 1/10 of the one-photoelectron peak) was determined. The results are summarized in table I.

The efficiency of the geometrical-match requirement between the trigger track and the energy cluster in the EMSDs was estimated as follows. Firstly, it was checked that the distance between the track impact point (determined by extrapolation from the last chamber in front of the EMSD) and the nearest energy cluster showed a Gaussian distribution in which the noise, coming from random hits, was negligible. Then, the efficiency was computed by looking at how many tracks did not have an associated energy cluster. The results for sandwich (SW) and lead-glass (LG) EMSDs are summarized separately in table I.

The efficiency of the geometrical-match requirement between the trigger track and the four hit wire clusters on the planes of the dE/dx chamber was

derived from the rate of intermediate missing planes, using for cleanness the sample of « pion » triggers. Only the configurations with the 2nd, the 3rd or the 4th plane missing were taken into account. The resulting efficiency was 0.944.

As already mentioned, the « pion » trigger $\overline{\mathrm{PH}}$ distribution in the $\mathrm{d}E/\mathrm{d}x$ chamber was used to evaluate the efficiency of the pluse-height cut for $\mathrm{e}^{\pm}$. The charged-hadron $\overline{\mathrm{PH}}$ spectrum was normalized and shifted so as to reproduce the prompt $\mathrm{e}^{\pm}$ spectrum (lower peak in fig. 7). The efficiency of the cut was in this way determined to be 0.78.

By using the same charged-hadron triggered events, the random vetoing introduced by the rejection criteria against narrow resolved $\mathrm{e}^{+}\mathrm{e}^{-}$ pairs was computed. The efficiency of this cut for the $\mathrm{e}^{\pm}$ trigger events was found to be 0.905.

When applying the filtering process to the trigger track, as found by the full reconstruction program, 10.4% of the events were rejected because the match of the track either with the energy cluster in the EMSDs or with the four hit wire clusters on the $\mathrm{d}E/\mathrm{d}x$ chamber planes was missing.

Other small inefficiencies, due to a bad tape-writing format or to an excess of hit wires in the MWPCs (not handled by the full reconstruction program), occurred during data taking and contributed with a factor equal to 0.934 to the total analysis efficiency.

A summary of all efficiencies is given in table I; the overall efficiency varied from 0.40 to 0.45 ($\pm$ 0.01) depending on the p_{T}^{*} value and the type of EMSD involved (sandwich or lead-glass).

8. – The invariant cross-section.

To evaluate the prompt $\mathrm{e}^{\pm}$ invariant cross-section, the centre-of-mass transverse momentum p_{T}^{*} was derived from the energy measured in the EMSDs, since no reliable momentum measurement was, in fact, expected in the almost-zero magnetic-field region covered by the lead-glass arrays.

The effect of the EMSDs' energy resolution on the $\mathrm{e}^{\pm}$ p_{T}^{*} spectrum was taken into account by an unfolding procedure based on the known energy dependence of the energy resolution for each EMSD element, and on a parametrization of the $\mathrm{e}^{\pm}$ p_{T}^{*} spectrum derived from the charge-averaged pion spectrum shape [8] (*). The total background contamination, which was obtained by introducing the same inefficiencies as for real data in the Monte Carlo results of sect. **6**, was then subtracted from the unfolded p_{T}^{*} spectrum. Finally,

(*) This unfolding procedure introduces into the experimental data a point-to-point correlation whose range, determined by the experimental energy resolution, varies slowly with energy. This effect can clearly be observed in fig. 12 to 14, in which the point-to-point fluctuations are obviously smaller than those expected from statistics.

after correction for the total e± detection efficiency, the invariant cross-section as a function of p_T^* was computed separately for positive and negative electrons: for the latter, the Compton background contribution was subtracted.

No data below $p_T^* = 1.0$ GeV/c were used, since only above this value was the efficiency of the EMSDs' hardware threshold at a maximum and the confidence level of the background evaluation satisfactory. In order to investigate a possible charge asymmetry effect, the difference in invariant cross-section between positrons and electrons was studied as a function of p_T^* (fig. 12). No evidence of charge asymmetry was found, the weighted average of the above difference in the p_T^* range from 1.0 to 3.0 GeV/c being 0.035 ± 0.038.

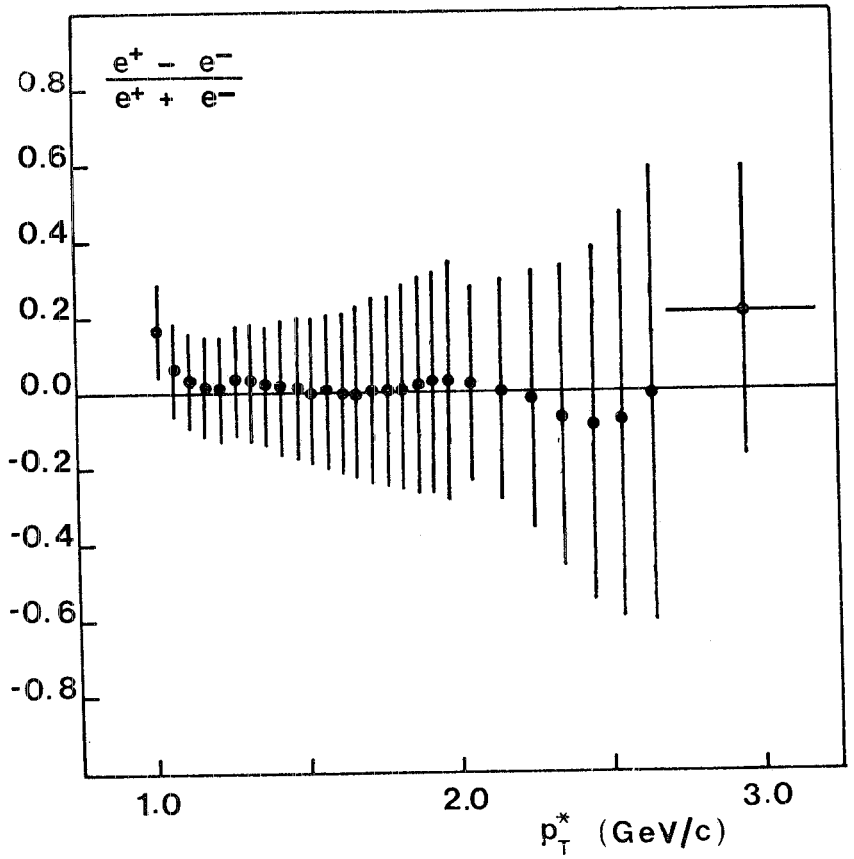

Fig. 12. – Charge asymmetry as a function of p_T^* for the final e± sample.

The charge-averaged invariant cross-section for prompt e± was then computed (table III); in fig. 13 its dependence on p_T^* is shown together with the results of a previous experiment ([1]) performed in the same kinematical region at the ISR. The behaviour of the charge-averaged pion cross-section ([8]) multiplied by 10^{-4} is also shown. This allows us to derive the e/π ratio *vs.* p_T^*.

TABLE III. – *The charge-averaged invariant cross-section for inclusive* $e^{\pm}$ *production at* $\sqrt{s} = 62.2$ GeV *as a function of* p_T^*.

p_T^* (GeV/c)	$E\,d^3\sigma/dp^3$ ($cm^2/(GeV)^2$)	p_T^* (GeV/c)	$E\,d^3\sigma/dp^3$ ($cm^2/(GeV)^2$)
1.022	$(6.83 \pm 0.88) \cdot 10^{-32}$	1.973	$(1.50 \pm 0.49) \cdot 10^{-33}$
1.072	$(5.86 \pm 0.74) \cdot 10^{-32}$	2.041	$(1.16 \pm 0.30) \cdot 10^{-33}$
1.122	$(4.70 \pm 0.60) \cdot 10^{-32}$	2.142	$(8.05 \pm 2.36) \cdot 10^{-34}$
1.172	$(3.64 \pm 0.49) \cdot 10^{-32}$	2.242	$(5.51 \pm 1.88) \cdot 10^{-34}$
1.222	$(2.81 \pm 0.40) \cdot 10^{-32}$	2.342	$(3.77 \pm 1.50) \cdot 10^{-34}$
1.272	$(2.23 \pm 0.34) \cdot 10^{-32}$	2.442	$(2.60 \pm 1.21) \cdot 10^{-34}$
1.322	$(1.75 \pm 0.28) \cdot 10^{-32}$	2.542	$(1.87 \pm 0.99) \cdot 10^{-34}$
1.372	$(1.41 \pm 0.24) \cdot 10^{-32}$	2.642	$(1.37 \pm 0.82) \cdot 10^{-34}$
1.422	$(1.13 \pm 0.20) \cdot 10^{-32}$	2.743	$(1.01 \pm 0.68) \cdot 10^{-34}$
1.472	$(9.18 \pm 1.74) \cdot 10^{-33}$	2.843	$(7.38 \pm 5.71) \cdot 10^{-35}$
1.522	$(7.55 \pm 1.50) \cdot 10^{-33}$	2.943	$(5.08 \pm 4.68) \cdot 10^{-35}$
1.572	$(6.18 \pm 1.30) \cdot 10^{-33}$	3.043	$(3.34 \pm 3.78) \cdot 10^{-35}$
1.623	$(5.17 \pm 1.14) \cdot 10^{-33}$	3.143	$(2.14 \pm 3.06) \cdot 10^{-35}$
1.673	$(4.28 \pm 1.00) \cdot 10^{-33}$	3.294	$(1.06 \pm 1.24) \cdot 10^{-35}$
1.723	$(3.56 \pm 0.88) \cdot 10^{-33}$	3.597	$(7.44 \pm 8.89) \cdot 10^{-36}$
1.773	$(2.99 \pm 0.78) \cdot 10^{-33}$	3.900	$(6.14 \pm 7.03) \cdot 10^{-36}$
1.823	$(2.50 \pm 0.69) \cdot 10^{-33}$	4.202	$(3.41 \pm 4.92) \cdot 10^{-36}$
1.873	$(2.12 \pm 0.62) \cdot 10^{-33}$	4.504	$(0.93 \pm 2.65) \cdot 10^{-36}$
1.923	$(1.79 \pm 0.55) \cdot 10^{-33}$	4.806	$(2.05 \pm 4.57) \cdot 10^{-36}$

9. – Conclusions.

The e/π ratio, as a function of p_T^*, is presented in fig. 14 and table IV; the weighted average in the p_T^* range from 1.0 to 3.0 GeV/c is $(1.58 \pm 0.06) \cdot 10^{-4}$.

Statistical errors and systematic errors in the detection efficiency and the background subtraction were taken into account in computing the $e^{\pm}$ cross-section (fig. 12 to 14). Other systematic errors originating from uncertainty in the luminosity measurement ($\pm 5\%$) and the accuracy of the absolute EMSD energy calibration ($\pm 5\%$) would result in a total normalization uncertainty of about $\pm 30\%$.

In order to compare our results with previous ISR experiments ([1,2]), at similar centre-of-mass energies, the following remarks are needed:

i) the ACHMNR data ([2]) are not corrected for a systematic effect which goes up to about $+ 33\%$; this means that the e/π ratio measured by this group is smaller than the true value;

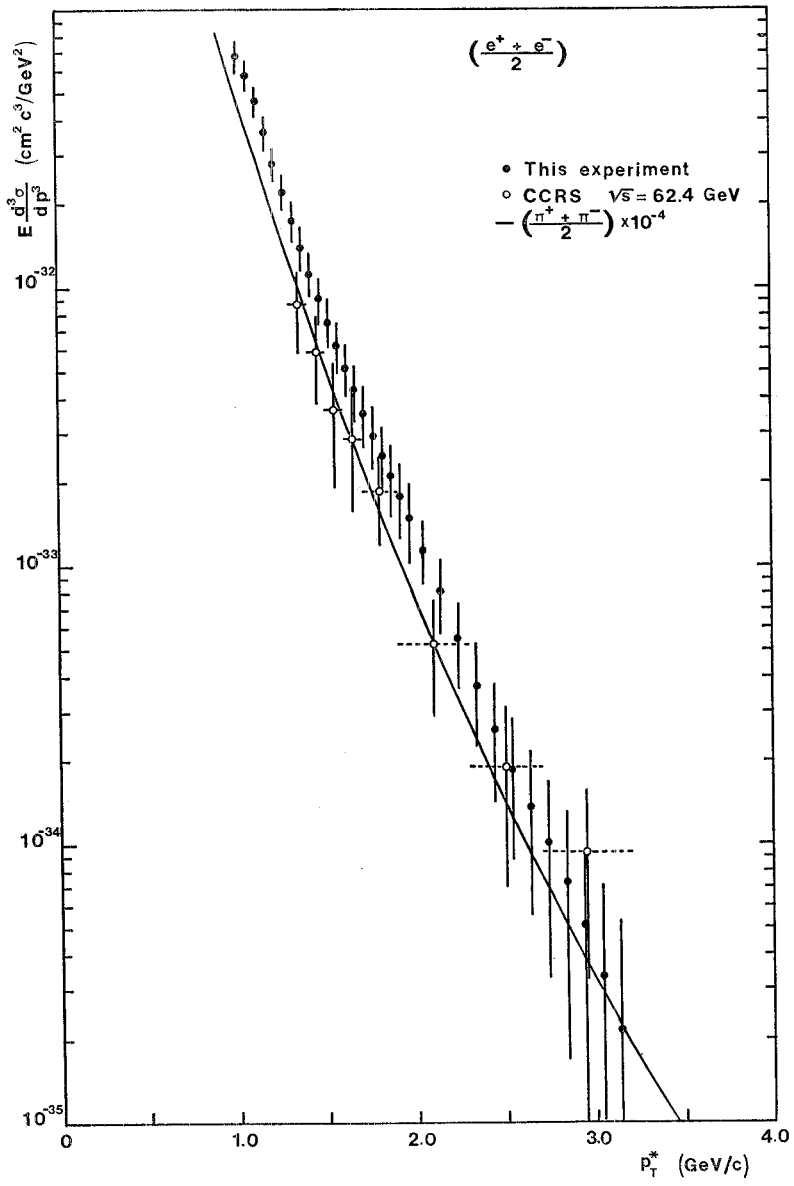

Fig. 13. – Prompt e± charge-averaged invariant cross-section as a function of p_T^* obtained in this experiment (black circles) and in a previous ISR experiment [1] (CCRS Collaboration: open circles) at $\sqrt{s} = 62.4$ GeV in the same kinematical region. The full line represents the fit [8] to the charge-averaged inclusive pion cross-section at 90° multiplied by 10^{-4}. Notice that only statistical errors are shown for the CCRS data points.

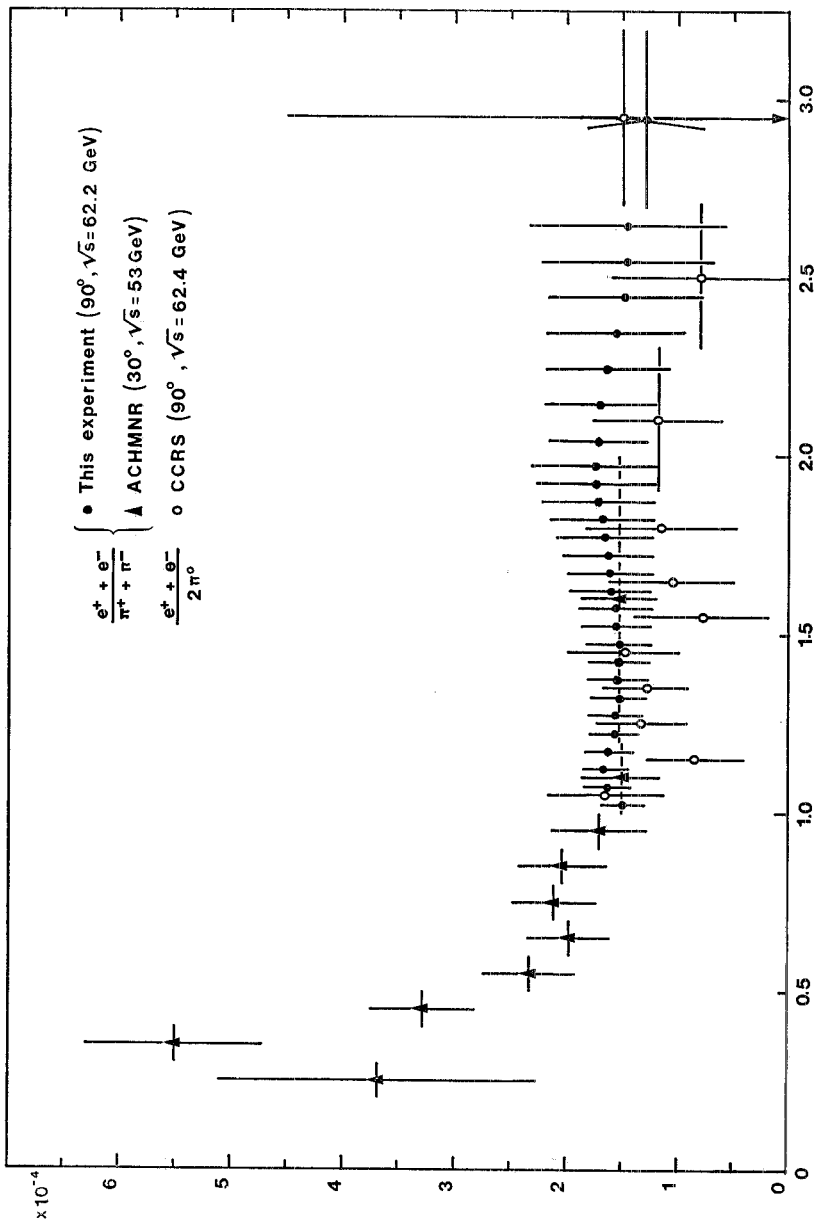

Fig. 14. – Charge-averaged e/π ratio measured in this experiment (black circles) as a function of p_T^*. The same fit [8] to the inclusive pion cross-section as that of fig. 13 was used to compute this ratio. Also shown are the results of two previous ISR experiments: one [2] at 30° and $\sqrt{s} = 53$ GeV (ACHMNR Collaboration: black triangles), and the other [1] at 90° and $\sqrt{s} = 62.4$ GeV (CCRS Collaboration: open circles). For the latter, the ratio of the electron to the π^0 rate, which was measured in the same experiment, is presented.

TABLE IV. – *The charge-averaged ratio* $[(e^+ + e^-)/(\pi^+ + \pi^-)] \cdot 10^4$ *as a function of* p_T^*, *at* $\sqrt{s} = 62.2$ GeV.

p_T^* (GeV/c)	$(e/\pi) \cdot 10^4$	p_T^* (GeV/c)	$(e/\pi) \cdot 10^4$
1.022	1.49 ± 0.19	1.723	1.63 ± 0.40
1.072	1.63 ± 0.20	1.773	1.66 ± 0.43
1.122	1.66 ± 0.21	1.823	1.68 ± 0.46
1.172	1.62 ± 0.22	1.873	1.72 ± 0.50
1.222	1.57 ± 0.23	1.923	1.74 ± 0.53
1.272	1.56 ± 0.23	1.973	1.75 ± 0.57
1.322	1.53 ± 0.25	2.041	1.72 ± 0.44
1.372	1.54 ± 0.26	2.142	1.70 ± 0.50
1.422	1.53 ± 0.27	2.242	1.64 ± 0.56
1.472	1.53 ± 0.29	2.342	1.56 ± 0.62
1.522	1.55 ± 0.31	2.442	1.48 ± 0.69
1.572	1.56 ± 0.33	2.542	1.46 ± 0.77
1.623	1.60 ± 0.35	2.642	1.46 ± 0.87
1.673	1.62 ± 0.38	2.943	1.30 ± 0.52

ii) the CCRS data [1] are affected by an overall systematic error of $\pm 28\%$ on the inclusive $e^{\pm}$ measurement (fig. 13) and of $\pm 7.3\%$ on the e/π ratio (fig. 14).

As mentioned in the introduction, the quantity e/π is strictly correlated, especially in the high-p_T range, with the semi-leptonic decay of the heavy flavours produced in high-energy pp interactions. In the present study this quantity has been measured by using the same hardware and software set-up which is used to study the heavy-flavour production at the ISR. Our results are consistent with previous measurements, and, besides providing a new contribution to the further knowledge of this basic quantity in high-energy hadron physics, they represent an important overall consistency check of the hardware and software systems used.

* * *

We wish to acknowledge the cooperation of the ISR experimental support group, the SFM detector group, the DD Division on-line support group, and the CERN-Collège de France-Heidelberg-Karlsruhe and Annecy-CERN-Collège de France-Dortmund-Heidelberg-Warsaw Collaborations. Thanks are also due to the Brookhaven-CERN-Rome, the Aachen-CERN-Heidelberg-Munich and the CERN Columbia-Rockfeller Collaborations, from whom we borrowed the lead-glass counters.

Finally we wish to thank F. BEAUVAIS, J. BERBIES, N. BOIMOND, G. MOLINARI and E. STOCCO for their skilful work during the preparation, assembly and running stages of the experiment.

APPENDIX

Experimental estimate of the background of e^+e^- pairs.

Owing to the corrugated shape of the ISR vacuum chamber, the mean thickness of stainless steel traversed by photons varied from point to point in a periodic way. The minimum thickness was 0.2 mm, but the mean thickness, integrated over the source length and crossing angles, was 0.32 mm.

A Monte Carlo simulation of the vacuum pipe showed a periodic variation of the effective thickness which could be fitted by a simple sinusoidal function superimposed on a continuum. The period was 2.5 cm (the input period of the corrugation was deduced from the design figures of the vacuum chamber) and the amplitude of the modulation $(32 \pm 5)\%$ of the mean value.

e^+e^- pairs originating from external conversions in the pipe wall must have the same modulation; this effect was, in fact, found in the experimental data. The $e^\pm$ rate (of the final sample of events) as a function of the crossing-point position along the vacuum pipe is shown in fig. 15. The distribution could be fitted by a smooth function (continuum) plus a sinusoid.

A fit of this kind was applied to two sets of data: *a*) a sample of unresolved e^+e^- pairs, selected by means of their average pulse height ($\overline{PH}$) in the dE/dx chamber; *b*) the sample of finally selected prompt $e^\pm$ events. The results of these fits can be summarized as in table A1. A confirmation that a real effect

TABLE A1.

Fit parameter	Sample *a*	Sample *b*
period T (cm)	2.39 ± 0.03	2.42 ± 0.02
zero co-ordinate y_0 (cm)	0.91 ± 0.08	0.83 ± 0.06
amplitude (% of the mean)	12.3 ± 2.7	4.41 ± 0.65
χ^2/d.o.f.	60/77	90/77

was observed came from the stability of the period T and the zero co-ordinate y_0 in the two fits, implying that the « same » vacuum chamber was observed in the two samples of events.

The interpretation of these results is the following. In the first case (sample *a*) true unresolved e^+e^- pairs from external and internal (Dalitz) conversions were detected; internal-conversion $e^\pm$ cannot be affected by the modulation effect, therefore the fit to sample *a* allowed the evaluation of the upper limit of the ratio of external to external-plus-internal conversion, *i.e.*

$$\frac{\text{external conversion}}{(\text{external} + \text{internal})\ \text{conversion}} \leqslant \frac{12.3 \pm 2.7}{32 \pm 5} = (38 \pm 10)\% .$$

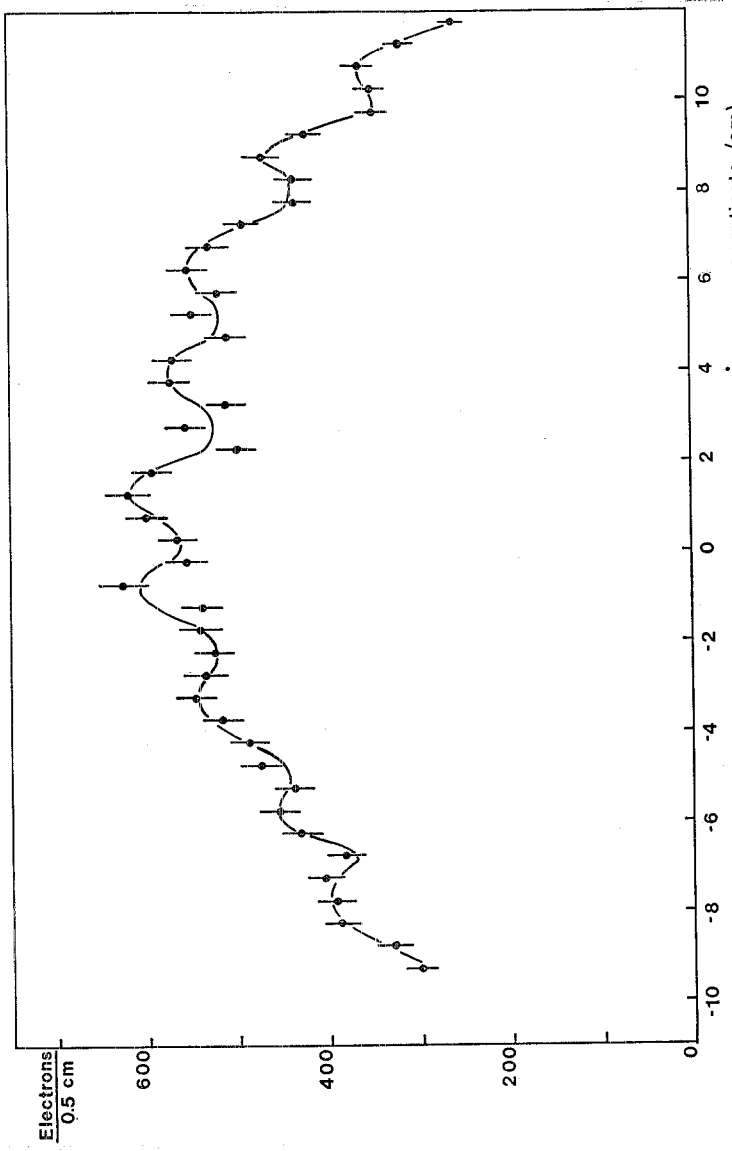

Fig. 15. – Final e± rate as a function of the crossing-point position (y co-ordinate) along the vacuum chamber, showing the modulation effect of the external-conversion pairs caused by the pipe corrugations.

In the second case (sample *b*) the amplitude of the modulation effect was a measurement of the residual external-conversion background in the final $e^{\pm}$ sample, *i.e.*

$$\frac{\text{external conversion}}{\text{total } e^{\pm} \text{ signal}} = \frac{4.41 + 0.65}{32 \pm 5} = (14 \pm 3)\% .$$

This experimental estimate compares well with the results of the Monte Carlo calculations (see sect. **6**) on the residual background from external conversions.

● RIASSUNTO

Si presenta una misura della produzione di $e^{\pm}$ « diretti » nelle interazioni protone-protone, effettuata agli ISR del CERN ad un valore dell'energia totale nel sistema del centro di massa $\sqrt{s} = 62.2$ GeV. Gli $e^{\pm}$ erano rivelati in un intervallo angolare di 35° intorno a $\theta = 90°$, con un impulso trasverso compreso tra 1.0 e 3.0 GeV/c.

Измерение мгновенного поперечного сечения $e^{\pm}$ рождения в протон-протонных соударениях при $\sqrt{s} = 62.2$ ГэВ.

Резюме (*). — Приводятся результаты измерений мгновенного рождения $e^{\pm}$ в протон-протонных соударениях в CERN ISR для энергии в системе центра масс $\sqrt{s}=62.2$ ГэВ, в угловой области $\Delta\theta=35°$ вблизи 90° и в области поперечных импульсов 1.0 ГэВ/с$\leqslant$ $\leqslant p_T^* \leqslant$ 3.0 ГэВ/с.

(*) *Переведено редакцией.*

CERN
SERVICE D'INFORMATION
SCIENTIFIQUE

M. BASILE, *et al.*
21 Ottobre 1981
Il Nuovo Cimento
Serie 11, Vol. **65** A, pag. 421-456